

**Preparation and Characterization of Co-Ni/Al<sub>2</sub>O<sub>3</sub> Catalyst for Steam Reforming of  
Acetic Acid**

by

Nor Amizah Binti Azid

Dissertation submitted in partial fulfilment of  
the requirements for the  
Bachelor of Engineering (Hons)  
(Chemical Engineering)

DECEMBER 2010

Universiti Teknologi PETRONAS  
Bandar Seri Iskandar  
31750 Tronoh  
Perak Darul Ridzuan

CERTIFICATION OF APPROVAL


**Preparation and Characterization of Co-Ni/Al<sub>2</sub>O<sub>3</sub> Catalyst for Steam Reforming of Acetic Acid**

by

Nor AmizahBintiAzid

A project dissertation submitted to the  
Chemical Engineering Programme  
UniversitiTeknologi PETRONAS  
in partial fulfilment of the requirement for the  
BACHELOR OF ENGINEERING (Hons)  
(CHEMICAL ENGINEERING)

Approved by,



(A.P DR ANITA BT RAMLI)


UNIVERSITI TEKNOLOGI PETRONAS

TRONOH, PERAK

December 2010

## CERTIFICATION OF ORIGINALITY

This is to certify that I am responsible for the work submitted in this project, that the original work is my own except as specified in the references and acknowledgements, and that the original work contained herein have not been undertaken or done by unspecified sources or persons.



NOR AMIZAH BINTI AZID

## ABSTRACT

The objectives of the Dissertation of the Final Year Project report is to record all relevant findings from literature reviews regarding the project of Preparation and Characterization of Co-Ni/Al<sub>2</sub>O<sub>3</sub> catalyst for steam reforming of Acetic Acid. The main objectives of this project is to study the methods of preparing the catalysts for steam reforming of acetic acid, to prepare the Co-Ni/Al<sub>2</sub>O<sub>3</sub> catalysts for steam reforming of acetic acid using impregnation method and to study the characteristics of Co-Ni/Al<sub>2</sub>O<sub>3</sub> catalysts. The background of the project is described in Chapter 1. Some literature researches were done in order to study the available methods for preparing catalyst supported on metal. There are three methods of introducing metal precursor, which is either by impregnation/ion exchange, co-precipitation and deposition precipitation. For this project, the catalysts were prepared by impregnation method and undergone several characterization measurements such as X-Ray Diffraction (XRD), Scanning Electron Microscopy (SEM) and Brunauer-Emmett-Teller method (BET). Further explanation for the methodology is discussed in Chapter 3. The results obtained from the characterization measurements were analyzed and discussed in Chapter 4. At the end of this project, it is found that the catalysts were successfully prepared by impregnation method and characterized for XRD, SEM and BET. However, catalyst testing was not done due to some technical problem. In Chapter 5, the conclusion and recommendations for this project is discussed.

## **ACKNOWLEDGEMENT**

I would like to express deepest gratitude to the Chemical Engineering Department of UniversitiTeknologi PETRONAS (UTP) for providing me this chance to undertake this remarkable final year project. I would like to thanks all parties that contribute to my research project directly or indirectly. A very special note of thanks to A.P Dr. Anita BintiRamli, who were always willing to help me and provided good support throughout. Your excellent support, patience and effective guidance have helped me completing my project.

I would like to thank the Final Year Project committee for arranging briefings and lecturer as support and knowledge to assist students in the project and report writing. The briefing and lectures were very helpful and insightful to me. Besides, I would like to thank all lecturers, technicians and graduate assistants from UniversitiTeknologi PETRONAS who had given me guidance throughout the period of the project.

Last but not least, my gratitude goes to my family and friends for providing me continuous support throughout the duration of this project.

## TABLE OF CONTENTS

CERTIFICATION OF APPROVAL.....	i
CERTIFICATION OF ORIGINALITY.....	ii
ABSTRACT.....	iii
ACKNOWLEDGEMENT.....	iv
TABLE OF CONTENTS .....	v
LIST OF FIGURE .....	vii
LIST OF TABLE .....	ix
CHAPTER 1: INTRODUCTION .....	1
1.1 BACKGROUND OF STUDY .....	2
1.2 PROBLEM STATEMENT .....	3
1.2.1 Problem Identification.....	3
1.2.2 Significant of the Project.....	4
1.3 OBJECTIVES AND SCOPE OF STUDY.....	4
1.3.1 Objectives.....	4
1.3.2 Scope of Study .....	5
1.3.3 The Relevancy of Project .....	5
1.3.4 Feasibility of the Project .....	6
CHAPTER 2: LITERATURE REVIEW .....	7
CHAPTER 3: METHODOLOGY .....	16
3.1 CATALYST PREPARATION .....	16
3.2 CATALYST CHARACTERIZATION.....	18
3.3 TOOLS REQUIRED.....	18
3.4 LIST OF CHEMICALS USED.....	18
CHAPTER 4: RESULT AND DISCUSSION .....	19
4.1 XRD Result .....	19
4.1.1 Sample 1 .....	20
4.1.2 Sample 2 .....	21
4.1.3 Sample 3 .....	22
4.1.4 Sample 4 .....	23
4.1.5 Sample 5 .....	24
4.1.6 Sample 6.....	25
4.1.7 Sample 7.....	26
4.1.8 Sample 8.....	27
4.1.9 Comparison of All XRD Results.....	28
4.1.10 Comparison with Literature Finding .....	29
4.2 SEM RESULT.....	30

4.3 EDX RESULT.....	35
4.3.1 Sample 1.....	35
4.4.1 Sample 1.....	36
4.4.2 Sample 2.....	38
4.4.3 Sample 3.....	40
4.4.4 Sample 4.....	42
4.4.5 Sample 5.....	44
4.4.6 Sample 6.....	46
CHAPTER 5: CONCLUSION.....	48
5.1 Recommendation.....	48
REFERENCES.....	
APPENDICES.....	
Appendix 1: EDX Result for sample 2.....	
Appendix 2: EDX Result for sample 3.....	
Appendix 3: EDX Result for sample 4.....	

## LIST OF FIGURE

Figure 1 Influences of the molar ratios of Ni and Co on the conversions of acetic acid. Experimental conditions: S/C mol ratio 7.5:1; LHSV = 5.1 h <sup>-1</sup> ; P = 1 atm .....	11
Figure 2 Mechanism of steam reforming .....	14
Figure 3 Flow Chart of Catalyst Preparation Methods .....	15
Figure 4 XRD Result for 100% Al <sub>2</sub> O <sub>3</sub> .....	20
Figure 5 XRD Result for 5%Ni/Al <sub>2</sub> O <sub>3</sub> .....	21
Figure 6 XRD Result for 5%Co/Al <sub>2</sub> O <sub>3</sub> .....	22
Figure 7 XRD Result for 2.5%Co2.5%Ni/Al <sub>2</sub> O <sub>3</sub> employing sequential impregnation method.....	23
Figure 8 XRD Result for 2.5%Ni2.5%Co/Al <sub>2</sub> O <sub>3</sub> employing sequential impregnation method.....	24
Figure 9 XRD Result for 2.5%Co2.5%Ni/Al <sub>2</sub> O <sub>3</sub> employing co-impregnation method.....	25
Figure 10 XRD Result for 1%Co4%Ni/Al <sub>2</sub> O <sub>3</sub> employing co-impregnation method.....	26
Figure 11 XRD Result for 4%Co1%Ni/Al <sub>2</sub> O <sub>3</sub> employing co-impregnation method .....	27
Figure 12 Comparison for XRD result for all samples.....	28
Figure 13 XRD result Ni/Al <sub>2</sub> O <sub>3</sub> from literature review.....	29
Figure 14 SEM Result for 5%Ni/Al <sub>2</sub> O <sub>3</sub> .....	30
Figure 15 SEM Result for 2.5%Ni2.5%Co/Al <sub>2</sub> O <sub>3</sub> employing sequential impregnation method .....	30
Figure 16 SEM Result for 2.5%Co2.5%Ni/Al <sub>2</sub> O <sub>3</sub> employing sequential impregnation method.....	31
Figure 17 SEM Result for 2.5%Co2.5%Ni/Al <sub>2</sub> O <sub>3</sub> employing co-impregnation method.....	31
Figure 18 SEM Result for 5%Ni/Al <sub>2</sub> O <sub>3</sub> .....	32
Figure 19 SEM Result for 2.5%Ni2.5%Co/Al <sub>2</sub> O <sub>3</sub> employing sequential impregnation method.....	32
Figure 20 SEM Result for 2.5%Co2.5%Ni/Al <sub>2</sub> O <sub>3</sub> employing sequential impregnation method.....	33
Figure 21 SEM Result for 2.5%Co2.5%Ni/Al <sub>2</sub> O <sub>3</sub> employing co-impregnation method.....	33
Figure 22 EDX Result for 5%Ni/Al <sub>2</sub> O <sub>3</sub> .....	35
Figure 23 Isotherm Linear Plot for Aluminum Oxide.....	36
Figure 24 Isotherm Linear Plot for 5%Ni/Al <sub>2</sub> O <sub>3</sub> .....	38
Figure 25 Isotherm Linear Plot for 5%Co/Al <sub>2</sub> O <sub>3</sub> .....	40
Figure 26 Isotherm Linear Plot for 2.5%Co2.5%Ni/Al <sub>2</sub> O <sub>3</sub> employing sequential method.....	42



Figure 27 Isotherm Linear Plot for 2.5%Ni2.5%Co/Al <sub>2</sub> O <sub>3</sub> employing sequential method.....	44
Figure 28 Isotherm Linear Plot for 2.5%Ni2.5%Co/Al <sub>2</sub> O <sub>3</sub> employing co-impregnation method .....	46

## LIST OF TABLE

Table 1 Influences of the molar ratio of Ni and Co on selectivities to the products....	11
Table 2 Composition of commercial steam reforming catalysts.....	13
Table 3 List of Chemicals used.....	18
Table 4 SEM results for Sample 1, Sample 2, Sample 3 and Sample 4 under 5000x magnification.....	30
Table 5 SEM results for Sample 1, Sample 2, Sample 3 and Sample 4 under 10000x magnification.....	32
Table 6 BET result analysis for 100% Al <sub>2</sub> O <sub>3</sub> .....	37
Table 7 BET result analysis for 5%Ni/ Al <sub>2</sub> O <sub>3</sub> .....	39
Table 8 BET result analysis for 5%Co/Al <sub>2</sub> O <sub>3</sub> .....	41
Table 9 BET result analysis for 2.5%Co2.5%Ni/Al <sub>2</sub> O <sub>3</sub> .....	43
Table 10 BET result analysis for 2.5%Ni2.5%Co/Al <sub>2</sub> O <sub>3</sub> employing sequential method.....	45
Table 11 BET result analysis for 2.5%Ni2.5%Co/Al <sub>2</sub> O <sub>3</sub> employing co-impregnation method.....	47

# CHAPTER 1

## INTRODUCTION

Living in the 21<sup>st</sup> century, the world has developed various kinds of advanced technologies with high requirement of energy. As time goes by, the world's dependence on energy becomes crucial as to sustain the requirement of technology development. This phenomenon results in depleting of world's primary energy – fossil fuel. Fossil fuels offer about 66% of the world's electrical power, and 95% of the world's total energy demands including heating, transport, electricity generation and other uses. (Noonan, 1996) Looking at how crucial energy is in our lives, the world is now focusing on renewable energy development to sustain the current demand for energy consumption. Traditionally, hydrogen is obtained from fossil fuels such as natural gas, naphtha, and coal. However, due to environmental issues and high dependence on depleting fossil fuels, the world's focus is now turned to producing hydrogen from alternative resources. Many researches are being conducted worldwide to develop the production of hydrogen via developed renewable energy technologies. Currently, there are several routes available for producing hydrogen from alternative fuels, and the most attractive is to produce hydrogen from biomass via pyrolysis mechanism using renewable technologies. Some methods for producing hydrogen have been investigated, which is gasification or pyrolysis of biomass to produce bio-oil before converting the bio-oil into hydrogen via steam reforming (Hu, 2007). Steam reforming of bio-oil from biomass pyrolysis is being developed for producing hydrogen using various catalysts. Current studies done involved the methods of catalyst preparation, catalyst characterization and the effect of catalyst preparation methods on the hydrogen yield. Some studies include the preparation of single metal catalyst on support while some other studies include the preparation of bi-metal catalyst without support. In this project, the catalyst preparation method and Ni-Co ratio is being studied to observe the effect to catalyst characteristics.

## 1.1 BACKGROUND OF STUDY

Recently, hydrogen is being considered as an environmentally friendly source of energy for automotive as well as stationary applications. Hydrogen is recognized as a clean fuel and energy carrier in the future economy because it has the significant advantage of producing no air or other pollutants when transforming to energy. At present, most of the hydrogen is produced from fossil fuels such as natural gas, naphtha and coal. Due to environmental pollution and high dependence on fossil fuel, the world is now focusing on producing hydrogen from alternative fuels such as biomass. The production of hydrogen from biomass is regarded as one of the main renewable technologies for it can achieve the zero emissions of carbon dioxide and make us less dependent on fossil fuels for power and transports (Czernik, 1999). Therefore, some methods of producing hydrogen from biomass are being investigated, which is (i) gasification/water-gas shift technology or (ii) flash pyrolysis of biomass followed by steam reforming of biomass products.

According to Czernik (1999), hydrogen content in biomass is only 6-6.5%, thus direct production of hydrogen from biomass by gasification/water-gas shift technology is unfavorable economically, except for very low-cost feed stocks and very large plant. Other than that, Davidian(2008) said“Although hydrogen can be produced by direct gasification of solid biomass, the catalysts poisoning by liquid tars and solid chars formed during the process remains a major issue”. Besides, direct utilization of solid biomass has low energetic density, which leads to high transportation costs. Such issues can be overcome by first liquefying the biomass through a fast pyrolysis process.

Therefore, we are investigating the second method in this project, which combines two stages; fast pyrolysis of biomass to generate a liquid product named bio-oil, then followed by the catalytic steam reforming of the bio-oil or its fractions to produce a gaseous stream rich in hydrogen. Czernik (1999) says that this integrated process in

which biomass is partially used to produce valuable materials or chemicals, while the residual fractions are utilized for the hydrogen generation may be economically viable in today's energy market.

The molecular composition of pyrolysis oil varies significantly with the type of biomass and the operating conditions of the pyrolysis process, such as pyrolysis severity and media. The major components of pyrolysis are oxygenates belonging to the groups of acids, aldehydes, alcohols, ketones and substituted furans derived from cellulose and hemi-cellulose as well as phenolic and cyclic oxygenates derived from lignin. Therefore, "many studies were restricted to model compounds of bio-oil such as acetic acid, alcohols, phenol, aldehydes and sugars." (Davidian, 2008) However, these molecules are not thermally stable at typical reforming temperatures, while some of them may not even be stable at much lower temperatures. Thus, there is a significant competition between catalytic reforming reactions and thermal decomposition for most oxygenates (Basaggianis, 2006).

## **1.2 PROBLEM STATEMENT**

### **1.2.1 Problem Identification**

Steam reforming is a renewable technology in producing hydrogen for environmentally friendly and sustainable supply of energy. This new technology includes the flash pyrolysis of biomass to bio-oil followed by steam reforming of the bio-oil to generate hydrogen. As the major components of pyrolysis – bio-oil (such as acetic acid) are oxygenates, which are thermally instable, there might be a significant competition between catalytic reforming reactions and thermal decomposition of oxygenates. Thus, a study about the catalyst activities and selectivity is required to understand the reaction network of both the thermally induced cracking/decomposition and the catalytic steam reforming.

Based on some researches from literature reviews, the author has come out with some problem statements; (i) how does the preparation method affect the catalyst performance in steam reforming of acetic acid? and (ii) does the Ni/Co ratio have significant effect on the catalyst performance?

To find out the answer, the author has conducted some experiments varying the catalyst preparation methods to see the effect of the sequence of adding the support into catalyst metal solution. Besides, the author has manipulated the Ni/Co ratio when preparing the catalysts.

### **1.2.2 Significant of the Project**

There is a lot of study being done nowadays regarding the steam reforming of acetic acid using various catalysts such as Pt/ZrO<sub>2</sub>, Ni-Co, Ni/La<sub>2</sub>O<sub>3</sub>, Ni/Al<sub>2</sub>O<sub>3</sub> and Co/Al<sub>2</sub>O<sub>3</sub>. In this project, the catalyst selectivity and activities will be studied for steam reforming using Ni-Co/Al<sub>2</sub>O<sub>3</sub> to compare the findings with the studies done using other catalysts earlier. The findings of this project are expected to be better than the ones done before as the catalyst used in this project is bimetallic catalysts – Ni-Co supported on alpha Alumina (Ni-Co/ $\alpha$ -Al<sub>2</sub>O<sub>3</sub>)

## **1.3 OBJECTIVES AND SCOPE OF STUDY**

### **1.3.1 Objectives**

The objectives of this study are:

- i) To study the methods of preparing the catalysts for steam reforming of acetic acid
- ii) To prepare the Co-Ni/Al<sub>2</sub>O<sub>3</sub> catalysts for steam reforming of acetic acid using impregnation method

- iii) To study the characteristics of Co-Ni/Al<sub>2</sub>O<sub>3</sub> catalysts

### **1.3.2 Scope of Study**

The scope of study of this project is as outlined in the objectives above, includes the preparation of catalysts for steam reforming which is Co-Ni supported by  $\alpha$ -Al<sub>2</sub>O<sub>3</sub> (alpha Alumina). There are various methods of preparing the supported catalysts such as precipitation and impregnation. For preparing the  $\alpha$ -Al<sub>2</sub>O<sub>3</sub> supported Co-Ni catalysts, we employ the methods of impregnation of single metal catalyst as well as bimetal catalysts. The details of the methodology will be further discussed in Chapter 3, Methodology.

Once the catalysts were prepared, their characteristics will be studied, including X-ray diffraction spectra (XRD), Scanning Electron Microscopy (SEM), and Brunauer-Emmett-Teller method (BET). The prepared catalyst will be submitted for the measurements of characterization and the results obtained will be analyzed. The findings from the characterization will be further discussed in Chapter 4, Results and Discussion.

Besides, the effects of catalyst preparation's methods and Co-Ni ratio will be studied upon the production of hydrogen by steam reforming. The activities of catalysts were determined in terms of conversion of acetic acid and the selectivity to the products. The best condition will later be determined for optimum hydrogen production of steam reforming of acetic acid using Co-Ni/Al<sub>2</sub>O<sub>3</sub> catalysts.

### **1.3.3 The Relevancy of Project**

As the world is focusing on developing renewable energy such as fuel cell using hydrogen, this project of Preparation and Characterization of Co-Ni/Al<sub>2</sub>O<sub>3</sub> for Steam

Reforming of Acetic Acid is relevant in order to determine the best condition for optimum hydrogen production of steam reforming. As mentioned before, the hydrogen is produced by fossil fuels which emit green house gases and other air pollutants when combusted. Besides, the fossil fuels are depleting as time goes by. The technology of steam reforming is being developed for sustainable and clean energy supply for current and future use. Thus, the study of the characteristics and activities of catalyst in this project will contribute to the optimum production of hydrogen gas by steam reforming. Perhaps the findings from this study can be commercialized and contribute to the industry and nationwide for clean and sustainable energy supply.

#### **1.3.4 Feasibility of the Project**

The project of Preparation and Characterization of Co-Ni/Al<sub>2</sub>O<sub>3</sub> for Steam Reforming of Acetic Acid is feasible to be completed within two semesters. This project involves the experiments to prepare and study the characteristics of Co-Ni/Al<sub>2</sub>O<sub>3</sub> catalysts. Besides, there will be some experiments to study the effects of Co-Ni ratio upon the production of hydrogen. Once the consumables are available in the lab, the experiment can be started with preparation of the catalysts and further study on the catalysts' characteristics and followed by the study of the Co-Ni ratio on the hydrogen production. Within two semesters, the author believes that she gets ample time to finish this project completely.



## CHAPTER 2

### LITERATURE REVIEW

Biomass is defined as any hydrocarbon material consisting of carbon, hydrogen, oxygen and nitrogen. Biomass resources include various natural and derived materials, such as woody and herbaceous species, wood wastes, agricultural and industrial residues, aquatic plants and algae etc. Biomass can be converted into useful energy sources such as hydrogen by (i) gasification/water-gas shift technology or (ii) flash pyrolysis of biomass followed by steam reforming of biomass products. According to Yaman (2003), direct combustion of biomass is unfavorable as it has too high content of moisture to perform stable combustion, contributing to highly changeable combustion rates. Thus, biomass pyrolysis is the best option to make use of its energy potential.

Pyrolysis of biomass can be described as the direct thermal decomposition of the organic matrix in the absence of oxygen to obtain products of solid, liquid and gas. Short residence time of pyrolysis of biomass at moderate temperatures has generally been used to obtain high yield of liquid products of pyrolysis, which is mainly bio-oil. According to Yaman (2003), the pyrolysis liquid products contain complex mixtures of oxygenated aliphatic and aromatic compounds. Methane ( $\text{CH}_4$ ), ethylene ( $\text{C}_2\text{H}_4$ ), propene ( $\text{C}_3\text{H}_6$ ), propane ( $\text{C}_3\text{H}_8$ ), methanol ( $\text{CH}_3\text{OH}$ ), acetic acid ( $\text{C}_2\text{H}_4\text{O}_2$ ), acetaldehyde ( $\text{C}_2\text{H}_4\text{O}$ ),  $\text{C}_4$ -hydrocarbons, carbon monoxide ( $\text{CO}$ ), carbon dioxide ( $\text{CO}_2$ ) and water ( $\text{H}_2\text{O}$ ) were designated as pyrolysis products. (Yaman, 2003)

Bio-oil is a complex mixture containing various aliphatic/aromatic oxygenates. The complexity of bio-oil has established the not straight forward requirements for a catalyst employed in steam reforming process. However, a more realistic approach is recognized – activity correlations based on studies using individual components present in bio-oil. Thus, we investigate steam reforming of acetic acid; one of the major components in bio-oil. The advantage of using acetic acid in this project is it is renewable and can be

easily obtained from biomass by fermentation. Acetic acid is produced by fermenting various substrates (starchy solution, sugar solutions or alcoholic foodstuffs) with *Acetobacter* bacteria. Other advantage of employing acetic acid is it is noninflammable; hence it is a safe hydrogen carrier. Furthermore, acetic acid can be easily converted to hydrogen with high selectivity at low temperature over effective catalysts such as Nickel-Cobalt (Ni-Co) (Hu, 2007). Up to now, there is a few catalysts have been investigated for steam reforming of acetic acid, such as platinum (Pt), rhodium (Rh) and palladium (Pd) based catalysts.

Currently, the world is focusing on producing hydrogen from renewable biomass feed stocks as an alternative to fossil fuels because it is essentially zero net CO<sub>2</sub> impact. The proposed method of producing hydrogen from biomass combines two stages, fast pyrolysis of biomass to produce bio-oil and catalytic steam reforming of bio-oil to produce hydrogen and carbon dioxide. According to Czernik (1999), there are some advantages of this proposed method, which are (i) bio-oil is much easier to transport than solid biomass and therefore, pyrolysis and reforming can be carried out at different locations to improve the economics and (ii) the potential production and recovery of higher value added co-products from bio-oil that could significantly impact the economics of the entire process.

Steam reforming can be conducted with the entire bio-oil or with each of its fraction or with hemicelluloses fraction from steam-aqueous processing. From the previous study, by using commercial nickel catalyst, the hydrogen yield obtained approached at least 90% of those possible stoichiometric conversions. The oil fraction was injected into reactor in form of fine mist to reduce the undesired reaction of thermal decomposition of the volatile compounds in the oil (sugars and oligomers) before contacting to the steam reforming catalyst. The exhausted catalyst can be regenerated by steam or carbon dioxide gasification. However, the process needs to be optimized to determine the

operating conditions (temperature, steam to carbon ratio) that allows for maximum yields of hydrogen and minimum coke formation. (Czernik, 1999)

Acetic acid (AcOH) is used to investigate the process of steam reforming as it is one of the major components of bio-oil. In the investigation conducted by Takanabe's team, the mechanistic studies on steam reforming of acetic acid over platinum supported on zirconium oxide (Pt/ZrO<sub>2</sub>) catalyst were studied. An overall picture of the bi-functional mechanism is established for steam reforming of acetic acid, where both Pt and ZrO<sub>2</sub> participate in the reaction. According to Takanabe (2006), it is proposed that a bi-functional mechanism is involved in steam reforming of AcOH over supported Pt catalysts. In the study, both Pt and the ZrO<sub>2</sub> support participate in the catalysis – the activation of AcOH and H<sub>2</sub>O.

The reaction stoichiometry for the conversion of AcOH to hydrogen can be drawn as  $\text{CH}_3\text{COOH} + 2\text{H}_2\text{O} \rightarrow 2\text{CO}_2 + 4\text{H}_2$ . It was found that on Pt, AcOH is decomposed to release H<sub>2</sub>, CO, CO<sub>2</sub>, and CH<sub>4</sub> into the gas phase and to leave carbonaceous residue that potentially deactivates the Pt surface. The residue can be gasified with water, forming additional H<sub>2</sub> and CO<sub>2</sub> (steam reforming). Based on the assumption that ZrO<sub>2</sub> activates water to form hydroxyl groups, infrared (IR) spectra of  $\nu(\text{OH})$  region were measured when the Pt/ZrO<sub>2</sub> catalyst was exposed to water vapor. IR measurement confirmed that water is activated on the ZrO<sub>2</sub>, forming surface hydroxyl groups, which are consumed in the gasification of carbon species derived from AcOH. Based on observations, it is proposed that the reaction must occur at the Pt–ZrO<sub>2</sub> boundary sites (Takanabe, 2006). Carbon dioxide produced in the reaction will be absorbed by limestone for zero emission of CO<sub>2</sub> to the atmosphere.

Catalytic generation of hydrogen by steam reforming of acetic acid over a series of Ni–Co catalysts was studied by Xun Hu and Gongzuan Lu in 2007. The catalyst were

prepared by using co-precipitation method where the aqueous mixture solution of metal salts,  $\text{Ni}(\text{NO}_3)_2$ ,  $\text{Co}(\text{NO}_3)_2$  were added to a vigorously stirred solution of  $\text{Na}_2\text{CO}_3$  at room temperature. The precipitation then was filtered and washed before drying and calcining. The characterization of catalyst then was done for X-ray diffraction (XRD) measurement, X-ray photoelectron spectroscopy (XPS) measurements and specific surface area measurements. The effects of molar ratios of Ni and Co in catalysts, reaction temperature, liquid hourly space velocity (LHSV) and molar ratios of steam-to-carbon (S/C) were studied in detail over this catalyst.(Hu, 2007)

From the experiments conducted in investigation of steam reforming of acetic acid to hydrogen over Ni–Co metal catalyst, it showed that the activities of the catalysts increased with the increase of Co content and reached maximum at the ratio of 0.25:1 between Ni and Co. And at this ratio, the Ni–Co catalyst not only showed the superior performances at 623 K, but also in the whole temperature range studied (523 K – 823 K). For the steam reforming of acetic acid, single metal Ni and Co catalysts were also active, but it was clear that they were inferior to Ni–Co catalyst (0.25:1), both in terms of conversions of acetic acid and selectivities to the products. It could be observed that reaction temperature had significant influences on acetic acid conversions and selectivities to the products in the temperature range studied. Ni–Co catalyst could produce hydrogen via acetic acid steam reforming in relatively low temperature range of 623–823K effectively. LHSV had less effect on the reforming reactions, while reaction temperature and S/C had significant influence on the conversions of acetic acid and distributions of the products(Hu, 2007).

Figure 1 shows the influences of the molar ratios of Ni and Co on the conversions of acetic acid with experimental conditions of: S/C mol ratio 7.5:1; LHSV =  $5.1 \text{ h}^{-1}$ ; P = 1 atm. In the meanwhile, table 1 shows influences of the molar ratio of Ni and Co on selectivities to the products. These table and figure were obtained from a study conducted by Hu (2007).

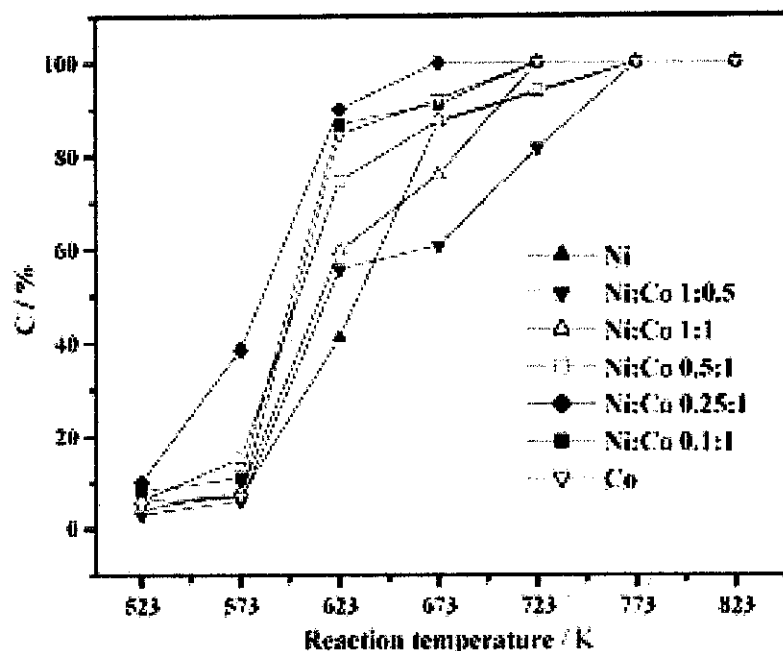


Fig. 1. Influences of the molar ratios of Ni and Co on the conversions of acetic acid. Experimental conditions: S/C mol ratio 7.5:1; LHSV = 5.1 h<sup>-1</sup>; P = 1 atm.

Figure 1: Influences of the molar ratios of Ni and Co on the conversions of acetic acid. Experimental conditions: S/C mol ratio 7.5:1; LHSV = 5.1 h<sup>-1</sup>; P = 1 atm

Table 1: Influences of the molar ratio of Ni and Co on selectivities to the products  
Influences of the molar ratios of Ni and Co on selectivities to the products

Catalysts	$S_{H_2}$ (%)	$S_{C_2H_4}$ (%)	$S_{CO}$ (%)	$S_{C_2H_2}$ (%)
Ni	93.4	3.1	1.2	95.6
Ni:Co (1:0.5)	95.1	1.1	0.21	97.3
Ni:Co (1:1)	95.7	2.2	0	95.8
Ni:Co (0.5:1)	96.2	0.96	0	97.9
Ni:Co (0.25:1)	96.3	0.94	0	98.1
Ni:Co (0.1:1)	95.9	1.5	0	95.7
Co	95.7	1.4	0	95.5

Experimental conditions— $T=573$  K; S/C mol ratio 7.5:1; LHSV = 5.1 h<sup>-1</sup>; P = 1 atm.

Acetic acid were used as a model compound to study its reaction network under steamreforming conditions over  $\text{Al}_2\text{O}_3$  and  $\text{La}_2\text{O}_3$ , and Ni catalyst supported on  $\text{La}_2\text{O}_3/\text{Al}_2\text{O}_3$  carrier, employing transient and steady-state techniques. In the study conducted by Basaggianis' team, the catalysts  $\text{La}_2\text{O}_3/\text{Al}_2\text{O}_3$  were synthesized by impregnating  $\gamma\text{-Al}_2\text{O}_3$  with  $\text{La}(\text{NO}_3)_3$  and for the supported Ni catalyst,  $\text{Ni}/(\text{La}_2\text{O}_3/\gamma\text{-Al}_2\text{O}_3)$ , was prepared by the wet impregnation method using  $\text{Ni}(\text{NO}_3)_2$  as the metal precursor. The catalysts were then characterized for X-ray diffraction (XRD) measurement, X-ray photoelectron spectroscopy (XPS) measurements and specific surface area measurements. In the experiment, the reaction scheme of steam reforming of acetic acid with respect to temperature was investigated by conducting series of transient experiments such as homogeneous reactions, reaction pattern over carriers and reaction scheme over  $\text{Ni}/(\text{La}_2\text{O}_3/\text{Al}_2\text{O}_3)$  catalyst. Besides, the experiments on catalyst performance under steady-state conditions and estimation of carbon deposition rate were also done. (Basaggianis, 2006)

From the study, it can be concluded that catalyst carriers such as  $\text{Al}_2\text{O}_3$  and  $\text{La}_2\text{O}_3$  interacts strongly with acetic acid and significant chemistry is taking place on the carrier itself. Besides, the presence of Ni active phase on the catalysts shifts activity toward lower temperatures. Ni promotes reforming reactions of acetic acid, as well as the water gas shift reaction. The overall reaction network of acetic acid steam reforming is highly complicated where thermal decomposition is taking place at intermediate temperatures, producing  $\text{CH}_4$ ,  $\text{CO}$ ,  $\text{CO}_2$  and  $\text{H}_2$ , while reforming reactions dominate at elevated temperatures, resulting in the formation of  $\text{H}_2$  and carbon oxides. Carbon deposition occurs at a high rate in the presence of  $\text{Al}_2\text{O}_3$ , and at a significantly lower rate in the presence of  $\text{La}_2\text{O}_3$ . This is due to the acidity of  $\text{Al}_2\text{O}_3$  which favors decomposition and polymerization reactions, resulting in the formation of significant carbonaceous species on the carrier, which are of the graphitic type. Carbon deposition rate is affected by reaction temperature, the acidity of the carrier and the  $\text{HAc}/\text{H}_2\text{O}$  ratio. Low reaction temperatures and high acetic acid-to-steam ratios favor carbon deposition on the catalyst surface. (Basaggianis, 2006)

The commercial catalysts were mainly used in those studies for steam reforming of hydrocarbons is summarized in Table 2. Table 2 shows the composition of commercial steam reforming catalysts. The typical order of activity of various catalysts tested in steam reforming of acetic acid was: Ni-based catalysts >> Pt > Rh > Pd ≈ Ru.

Table 2: Composition of commercial steam reforming catalysts

Producer	Feedstock	NiO	Al <sub>2</sub> O <sub>3</sub>	MgO	MgAl <sub>2</sub> O <sub>4</sub>	CaO	SiO <sub>2</sub>	K <sub>2</sub> O
BGC	Naphtha	79	20–21	–	–	–	–	0.75–3.3
ICI	Naphtha	22	26	11	–	13	16	7
ICI	Naphtha	10–25						1.5
ICI	Naphtha	22	26	11		13	16	7
ICI	C <sub>2</sub> /C <sub>3</sub>	+	+			+		
ICI	Natural gas	12	78	–	–	10	(0.1)	
ICI	Natural gas	15	70			13		1.5
Topsøe	Natural gas	15	–	–	85	–	(0.1)	<500 ppm
Topsøe	Natural gas/LPG	15	–	–	85	–	(0.1)	<500 ppm
Topsøe	Naphtha	34	12	54				
UCI	Natural gas	11–20						
UCI	Light hydrocarbons	15–25						
UCI	Light hydrocarbons	7–15						
UCI	C <sub>3</sub> CC <sub>4</sub> hydrocarbons	15	70–76			5–8		
UCI	C <sub>3</sub> CC <sub>4</sub> hydrocarbons	11	76–82			6–9		
UCI	C <sub>3</sub> CC <sub>4</sub> hydrocarbons	11	76–82			6–9		Unknown
BASF	Natural gas	15						
BASF	Naphtha	25	66			8	<0.2	1
BASF	Naphtha	20	32	11		16	14	7

Based on the table, we can see that Nickel is the main active component of the most of these catalysts. Although noble metals (Ru, Rh) are more effective than Ni and less susceptible to carbon formation, however, the catalysts are not common in industrial applications because of their cost (Garcia, 2000).

In other studies, Cobalt-promoted Ni/Al<sub>2</sub>O<sub>3</sub> is significantly more resistant to deactivation by carbon than nickel alone. The addition of Co to NiO-MgO catalysts has a beneficial effect by eliminating or significantly reducing the formation of filamental carbon on the catalyst during CO<sub>2</sub> reforming of methane (Choudary, 1998).

Catalytic reforming of hydrocarbons is assumed to proceed according to the mechanism proposed by Garcia(2000). Figure 2 shows the mechanism of steam reforming of acetic acid.

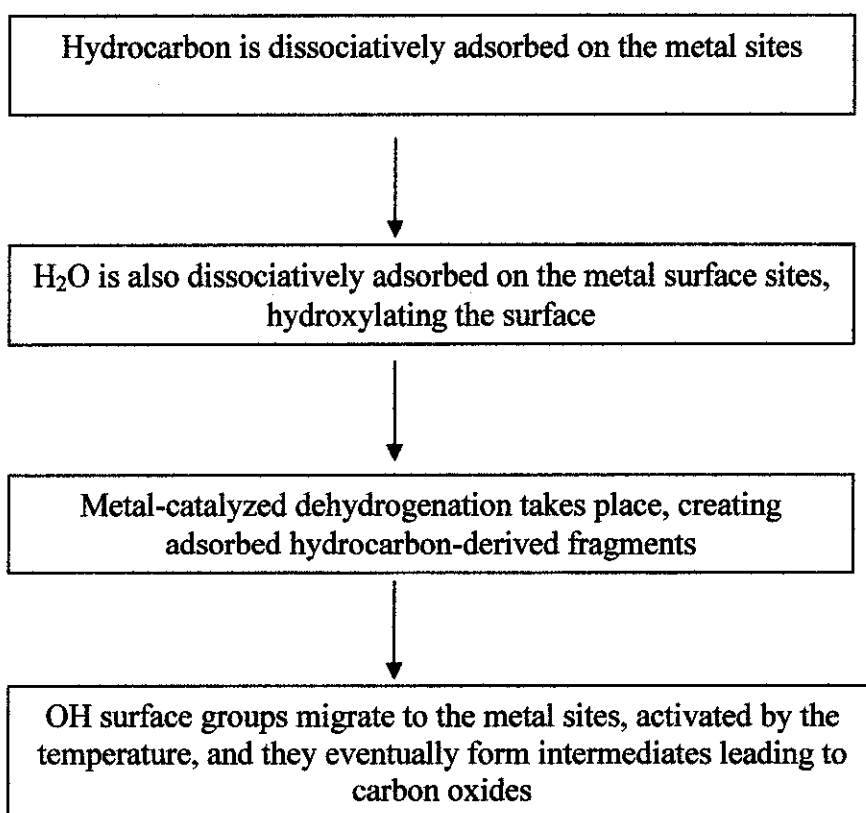


Figure 2: Mechanism of steam reforming



There are various methods to prepare the catalyst. Figure 3 shows the summary of available methods of preparing catalyst.

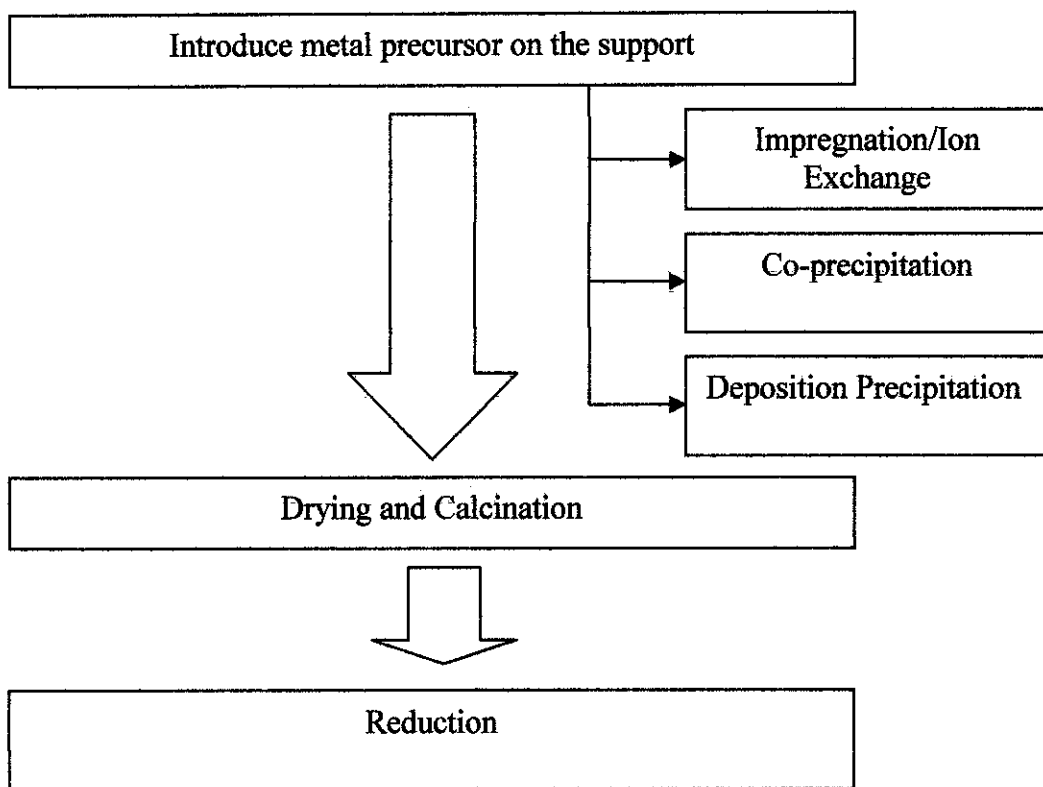


Figure 3: Flow Chart of Catalyst Preparation Methods

## **CHAPTER 3**

### **METHODOLOGY**

In this project, we are studying the effect of adding cobalt to the Ni/Al<sub>2</sub>O<sub>3</sub> catalyst to the activity and selectivity of catalyst for steam reforming of acetic acid. This project is started when the topics for Final Year Project (FYP) were released. Based on the title of the project, the literature reviews were done for author's better understanding and clearer view on what the project is all about. With sufficient information gained from literature readings, the research methodology was planned for the project.

Basically, this project is composed of several experiments designed for preparing the catalysts. After the preparation of catalyst is done, the catalyst will undergo some characterization techniques such as X-Ray Diffraction method (XRD), Scanning Electron Microscopy method (SEM), and Brunauer-Emmett-Teller method (BET) to examine solid surface and catalyst's properties both chemically and physically. The catalyst will then undergo steam reforming using acetic acid to study the effect of Ni/Co ratio upon catalyst performance.

#### **3.1 CATALYST PREPARATION**

The catalysts were prepared using wet impregnation method. Impregnation is the simplest way to prepare the catalyst supported on metal. There are two types of catalysts were prepared in this project, single metal catalyst and bi-metal catalyst. For single metal catalysts, there are two catalysts involved, namely Nickel supported on  $\alpha$ -Alumina (Ni/Al<sub>2</sub>O<sub>3</sub>) and Cobalt supported on  $\alpha$ -Alumina (Co/Al<sub>2</sub>O<sub>3</sub>). Bi-metal catalysts consist of Nickel supported on Cobalt/ $\alpha$ -Alumina (Ni-Co/Al<sub>2</sub>O<sub>3</sub>) and Cobalt supported on Nickel- $\alpha$ -Alumina (Co-Ni/Al<sub>2</sub>O<sub>3</sub>). Preparation of bi-metal catalyst is further divided into two methods, sequential impregnation and co-impregnation. For bi-metal catalysts, the ratio

of Ni/Co is varied to observe the effect upon the catalyst performance in steam reforming of Acetic Acid.

Catalyst preparation is started by introducing the metal precursor to the support of catalyst. For single metal catalyst, the metal precursor (Nickel or Cobalt) is introduced to the  $\text{Al}_2\text{O}_3$  support by impregnation method. The metal precursor is dissolved in sufficient amount of deionized water before adding the  $\text{Al}_2\text{O}_3$  support into the solution. The solution containing metal precursor and catalyst support were stirred for 6 hours on a magnetic stirrer. The solution was then dried at  $120^\circ\text{C}$  for 16 hours in a normal oven. The dried solution was then grinded before calcining in a rotary furnace at  $500^\circ\text{C}$  for 6 hours. The preparation of single metal is then completed.

For bi-metal sequential impregnation catalyst preparation, the first metal precursor is introduced to the support as in single metal catalyst preparation. The single metal catalyst prepared earlier will become the support of catalyst for the second metal precursor. The second metal precursor will be introduced to the support following the steps of preparing the single metal catalyst. The experiment will then be repeated for other Ni/Co ratio (1 to 5).

For bi-metal co-impregnation catalyst preparation, both metal precursors are dissolved in sufficient amount of deionized water before adding the support into the solution. The next step will be the same as in preparation of single metal catalyst.

### 3.2 CATALYST CHARACTERIZATION

These catalysts were characterized for X-ray diffraction (XRD), Scanning Electron Microscopy (SEM), and Brunauer-Emmett-Teller (BET) measurements. The results of each measurement were then analyzed. The findings will be further discussed in Chapter 4, Results and Discussion.

### 3.3 TOOLS REQUIRED

Catalyst preparation : Beaker, hot plate magnetic stirrer, magnetic bar, spatula, normal oven, rotary furnace

Catalyst characterization : Philips Xpert MPD, VG ESCALAB 210 spectrometer, Micromeritics ASAP-2010 apparatus

### 3.4 LIST OF CHEMICALS USED

Table 3: List of Chemicals used

Name of Chemical	Chemical Formula	Supplier	Molecular Weight
Aluminum Oxide	$\text{Al}_2\text{O}_3$	Fisher Scientific U.K Limited	101.96 g/mol
Nickel (II) Nitrate Hexahydrate	$\text{Ni}(\text{NO}_3)_2 \cdot 6\text{H}_2\text{O}$	R&M Marketing, Essex, U.K	290.81 g/mol
Cobalt (II) Nitrate Hexahydrate	$\text{Co}(\text{NO}_3)_2 \cdot 6\text{H}_2\text{O}$	MerkKGaA	291.04 g/mol

## CHAPTER 4

### RESULT AND DISCUSSION

#### 4.1 XRD RESULT

X-Ray Diffraction (XRD) method is used for catalyst characterization in this project because it allows a non-destructive structure analysis. In this project, XRD method is used for qualitative analysis to investigate the types of materials that compose a solid (the prepared catalysts).

The principle of XRD method is it works based on Bragg's Law. When a monochromatic x-ray beam with wavelength  $\lambda$  is incident on the lattice planes in a crystal at an angle  $\theta$ , diffraction occurs only when the distance traveled by the rays reflected from successive planes differs by a complete number  $n$  of wavelengths (Bragg's Law). Diffraction pattern contains a lot of structural information: the angular position of the reflections is related to the size and shape of the unit cell (the repeating unit of the crystal) while the intensities reflect the lattice symmetry and the electron density (practically the positions and types of atoms) within the unit cell (Perego, 1998).

### 4.1.1 Sample 1

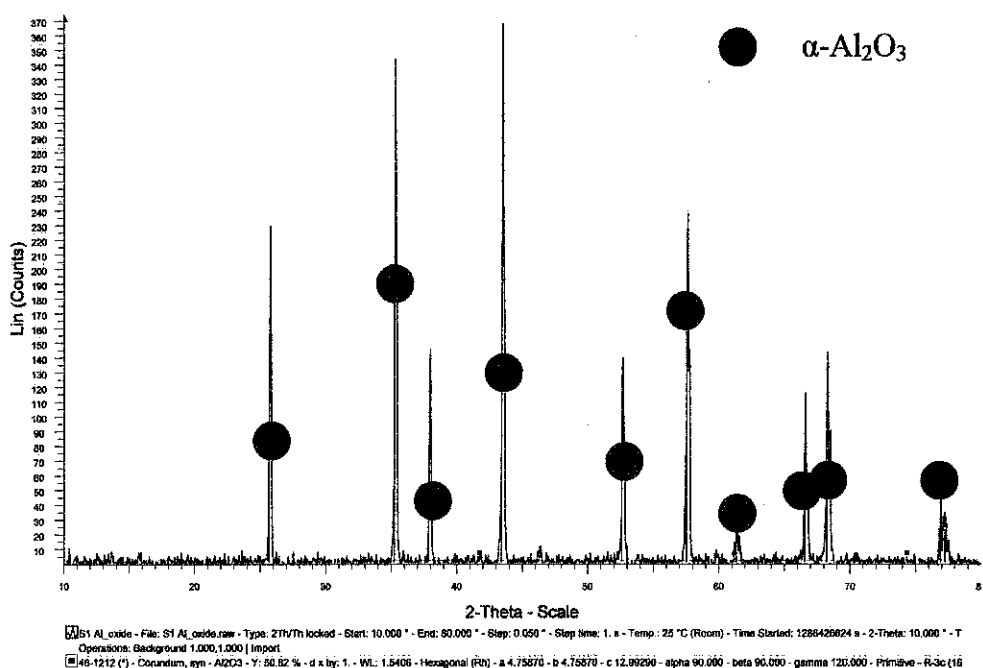


Figure 4: XRD Result for 100%  $\text{Al}_2\text{O}_3$

Figure 4 shows XRD result for  $\text{Al}_2\text{O}_3$  (100 wt%  $\text{Al}_2\text{O}_3$ ). Based on the graph, we can see some diffraction peaks appear at  $2\theta$  value of  $26^\circ$ ,  $35^\circ$ ,  $38^\circ$ ,  $43^\circ$ ,  $53^\circ$ ,  $58^\circ$ ,  $61^\circ$ ,  $67^\circ$ ,  $69^\circ$ , and  $77^\circ$ . The highest intensity is shown by diffraction peak at  $2\theta$  value of  $35^\circ$ . These diffraction peaks match the  $2\theta$  scale diffraction peak for Corundum Oxide, a crystalline form of  $\text{Al}_2\text{O}_3$ . The diffraction peaks show the presence of Corundum Oxide in the sample which conforms to the claim that the sample contains  $\text{Al}_2\text{O}_3$ . In the graph, diffraction peaks only match for Corundum because the sample contain 100 wt% of  $\text{Al}_2\text{O}_3$ .

## 4.1.2 Sample 2

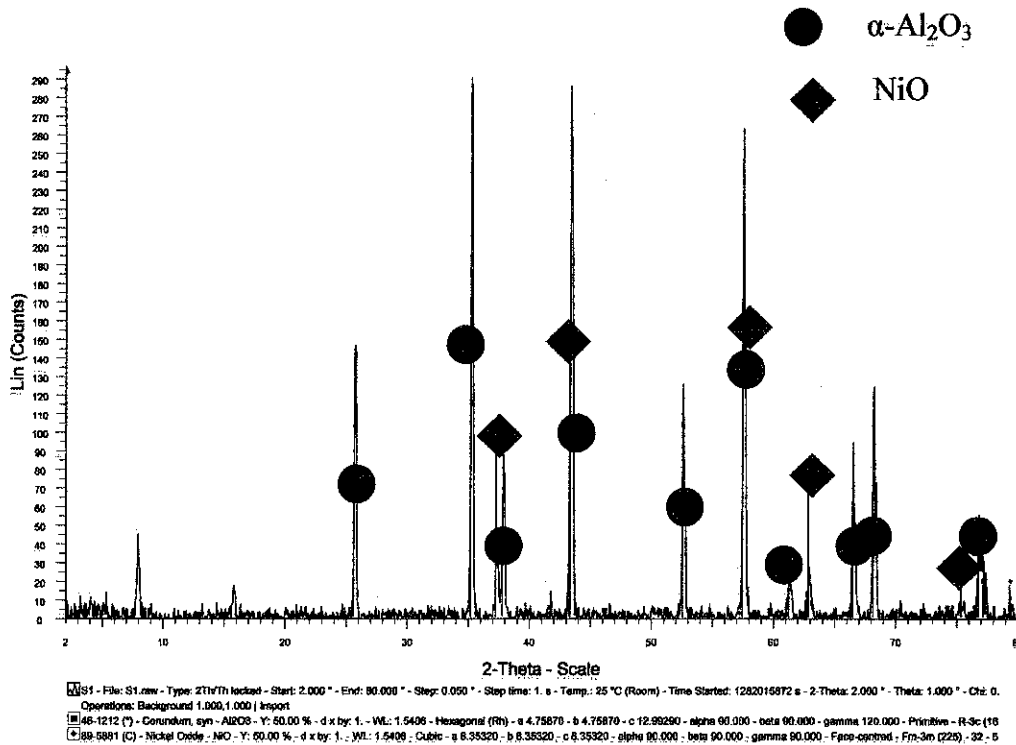


Figure 5: XRD Result for 5%Ni/Al<sub>2</sub>O<sub>3</sub>

Figure 5 shows XRD result for Ni/Al<sub>2</sub>O<sub>3</sub> (95 wt% Al<sub>2</sub>O<sub>3</sub>, 5 wt% Ni). Based on the graph, we can see some diffraction peaks appear at  $2\theta$  value of  $27^\circ$ ,  $35^\circ$ ,  $38^\circ$ ,  $43^\circ$ ,  $54^\circ$ ,  $58^\circ$ ,  $61^\circ$ ,  $66^\circ$ ,  $68^\circ$ , and  $78^\circ$ ; which match to Corundum Oxide. Besides, there are some diffraction peaks appear at  $2\theta$  value of  $36^\circ$ ,  $43^\circ$ ,  $57^\circ$ ,  $63^\circ$ ,  $66^\circ$ ,  $71^\circ$ ,  $75^\circ$ , and  $79^\circ$ ; which match to Nickel Oxide, NiO. The diffraction peaks show the presence of Corundum Oxide and NiO in the sample which conforms to the claim that the sample contains Ni/Al<sub>2</sub>O<sub>3</sub>. The highest intensity is shown by diffraction peak at  $2\theta$  value of  $35^\circ$  and  $45^\circ$  while the lowest intensity is shown by diffraction peak at  $2\theta$  value of  $70.5^\circ$ . The diffraction peaks with high intensity shows the amount of crystalline components detected in the sample. The higher the diffraction peak, the more crystalline phase of particular components present in the sample.

### 4.1.3 Sample 3

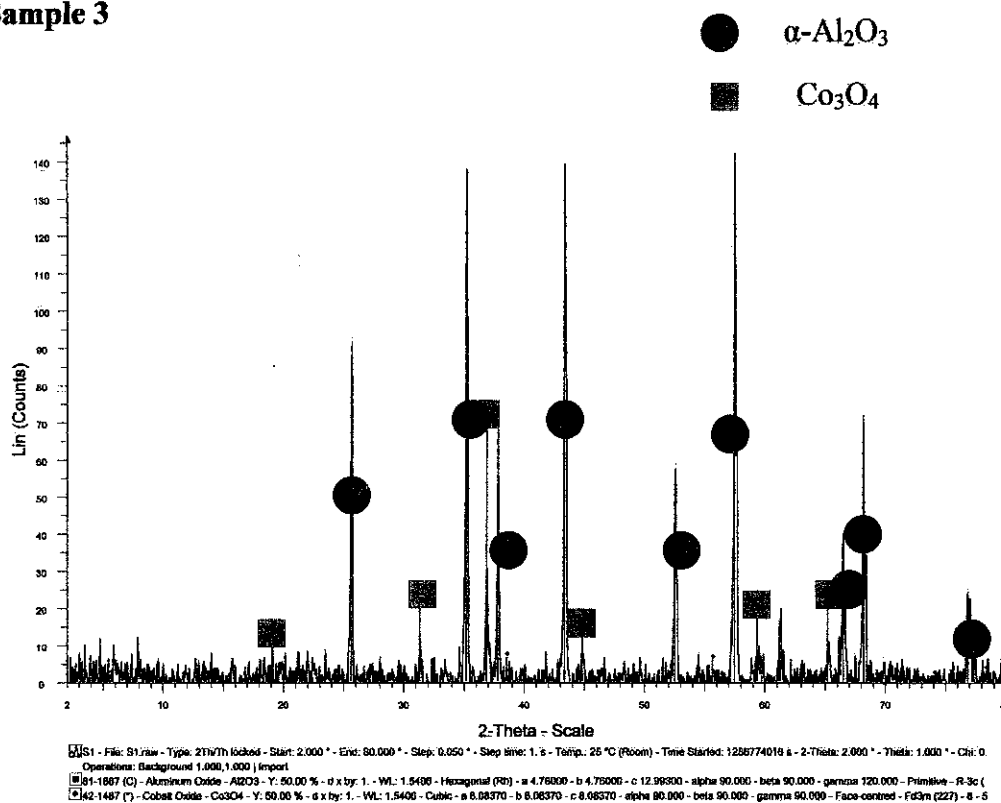


Figure 6: XRD Result for 5%Co/Al<sub>2</sub>O<sub>3</sub>

Figure 6 shows XRD result for Co/Al<sub>2</sub>O<sub>3</sub> (95 wt% Al<sub>2</sub>O<sub>3</sub>, 5 wt% Co). Based on the graph, we can see some diffraction peaks appear at  $2\theta$  value of 26.7°, 35°, 38°, 42°, 43°, 46°, 52.5°, 58°, 60°, 61°, 66°, 68°, 70°, 74° and 78°. These diffraction peaks match to Corundum Oxide. Besides, there are some diffraction peaks appear at  $2\theta$  value of 19°, 31°, 37°, 39°, 45°, 56°, 59°, 65°, 69°, 74°, 77°, and 78°. These diffraction peaks match to Cobalt Oxide, Co<sub>3</sub>O<sub>4</sub>. The diffraction peaks show the presence of Corundum Oxide and Co<sub>3</sub>O<sub>4</sub> in the sample which conforms to the claim that the sample contains Co/Al<sub>2</sub>O<sub>3</sub>. The highest intensity is shown by diffraction peak at  $2\theta$  value of 35° and 37° while the lowest intensity is shown by diffraction peak at  $2\theta$  value of 42°. The highest intensity appears at both Corundum Oxide and Cobalt Oxide diffraction peak, which shows that more crystalline phase of both components are detected in the sample.



#### 4.1.4 Sample 4

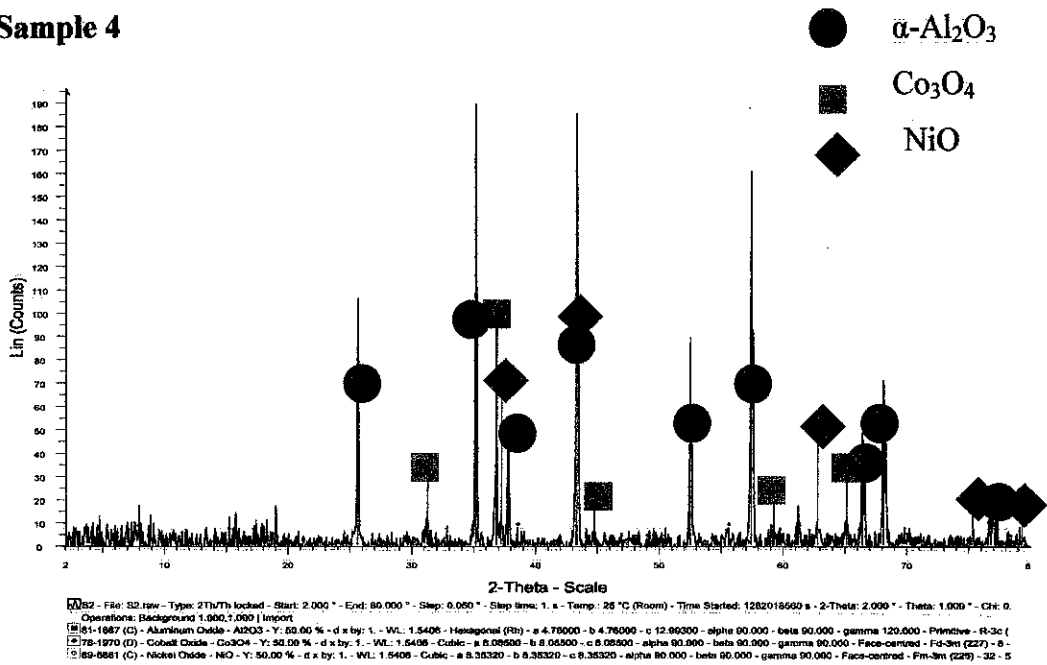


Figure 7: XRD Result for 2.5%Co2.5%Ni/Al<sub>2</sub>O<sub>3</sub> employing sequential impregnation method

Figure 7 shows XRD result for Co-Ni/Al<sub>2</sub>O<sub>3</sub> (95 wt% Al<sub>2</sub>O<sub>3</sub>, 2.5 wt% Co, 2.5% Ni). Based on the graph, we can see some diffraction peaks appear at  $2\theta$  value of  $26.7^{\circ}$ ,  $35^{\circ}$ ,  $38^{\circ}$ ,  $42^{\circ}$ ,  $43^{\circ}$ ,  $46^{\circ}$ ,  $52.5^{\circ}$ ,  $58^{\circ}$ ,  $60^{\circ}$ ,  $61^{\circ}$ ,  $66^{\circ}$ ,  $68^{\circ}$ ,  $70^{\circ}$ ,  $74^{\circ}$  and  $78^{\circ}$ , which match to Corundum Oxide. Besides, there are some diffraction peaks appear at  $2\theta$  value of  $19^{\circ}$ ,  $31^{\circ}$ ,  $37^{\circ}$ ,  $39^{\circ}$ ,  $45^{\circ}$ ,  $56^{\circ}$ ,  $59^{\circ}$ ,  $65^{\circ}$ ,  $69^{\circ}$ ,  $74^{\circ}$ ,  $77^{\circ}$ , and  $78^{\circ}$ ; which match to Cobalt Oxide, Co<sub>3</sub>O<sub>4</sub>. Besides, there are some diffraction peaks appear at  $2\theta$  value of  $18^{\circ}$ ,  $21^{\circ}$ ,  $31^{\circ}$ ,  $36^{\circ}$ ,  $37^{\circ}$ ,  $43^{\circ}$ ,  $47^{\circ}$ ,  $54^{\circ}$ ,  $57^{\circ}$ ,  $63^{\circ}$ ,  $66^{\circ}$ ,  $71^{\circ}$ ,  $75^{\circ}$ , and  $79^{\circ}$ ; which match to Nickel Oxide, NiO. The diffraction peaks show the presence of Corundum, Co<sub>3</sub>O<sub>4</sub> and NiO in the sample which conforms to the claim that the sample contains Co-Ni/Al<sub>2</sub>O<sub>3</sub>. The highest intensity is shown by diffraction peak at  $2\theta$  value of  $35^{\circ}$ ,  $37^{\circ}$  and  $43^{\circ}$  while the lowest intensity is shown by diffraction peak at  $2\theta$  value of  $18^{\circ}$ ,  $21^{\circ}$ ,  $31^{\circ}$ ,  $36^{\circ}$ ,  $46^{\circ}$ ,  $54^{\circ}$ ,  $57^{\circ}$ ,  $66^{\circ}$ , and  $71^{\circ}$ . The highest intensity appears at Corundum Oxide, Nickel Oxide and Cobalt Oxide diffraction peak, which shows that more crystalline phases of all components are detected in the sample at the specified intensity.

## 4.1.5 Sample 5

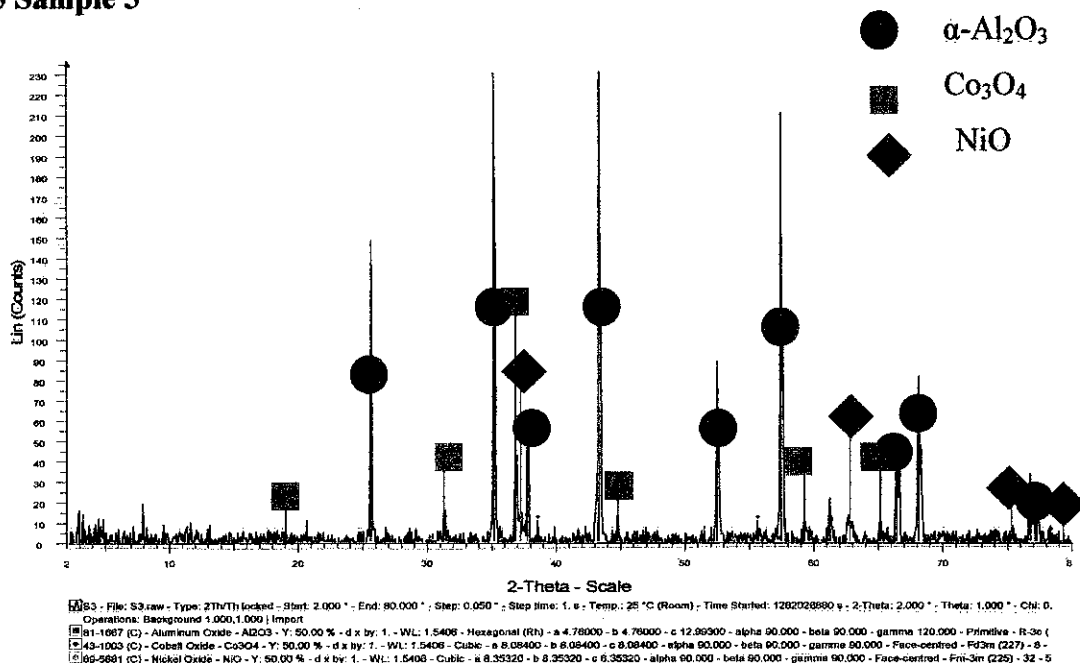


Figure 8: XRD Result for 2.5%Ni2.5%Co/Al<sub>2</sub>O<sub>3</sub> employing sequential impregnation method

Figure 8 shows XRD result for Ni-Co/Al<sub>2</sub>O<sub>3</sub> (95 wt% Al<sub>2</sub>O<sub>3</sub>, 2.5 wt% Co, 2.5% Ni). Based on the graph, we can see some diffraction peaks appear at  $2\theta$  value of  $26.7^\circ$ ,  $35^\circ$ ,  $38^\circ$ ,  $42^\circ$ ,  $43^\circ$ ,  $46^\circ$ ,  $52.5^\circ$ ,  $58^\circ$ ,  $60^\circ$ ,  $61^\circ$ ,  $66^\circ$ ,  $68^\circ$ ,  $70^\circ$ ,  $74^\circ$  and  $78^\circ$ ; which match to Corundum Oxide. Besides, there are some diffraction peaks appear at  $2\theta$  value of  $19^\circ$ ,  $31^\circ$ ,  $37^\circ$ ,  $39^\circ$ ,  $45^\circ$ ,  $56^\circ$ ,  $59^\circ$ ,  $65^\circ$ ,  $69^\circ$ ,  $74^\circ$ ,  $77^\circ$ , and  $78^\circ$ ; which match to Cobalt Oxide, Co<sub>3</sub>O<sub>4</sub>. Besides, there are some diffraction peaks appear at  $2\theta$  value of  $18^\circ$ ,  $21^\circ$ ,  $31^\circ$ ,  $36^\circ$ ,  $37^\circ$ ,  $43^\circ$ ,  $47^\circ$ ,  $54^\circ$ ,  $57^\circ$ ,  $63^\circ$ ,  $66^\circ$ ,  $71^\circ$ ,  $75^\circ$ , and  $79^\circ$ ; which match to Nickel Oxide, NiO. The diffraction peaks show the presence of Corundum, Co<sub>3</sub>O<sub>4</sub> and NiO in the sample which conforms to the claim that the sample contains Co-Ni/Al<sub>2</sub>O<sub>3</sub>. The highest intensity is shown by diffraction peak at  $2\theta$  value of  $35^\circ$ ,  $37^\circ$  and  $43^\circ$  while the lowest intensity is shown by diffraction peak at  $2\theta$  value of  $18^\circ$ ,  $21^\circ$ ,  $31^\circ$ ,  $36^\circ$ ,  $46^\circ$ ,  $54^\circ$ ,  $57^\circ$ ,  $66^\circ$ , and  $71^\circ$ . The highest intensity appears at Corundum Oxide, Nickel Oxide and Cobalt Oxide diffraction peak, which shows that more crystalline phases of all components are detected in the sample at the specified intensity.

## 4.1.6 Sample 6

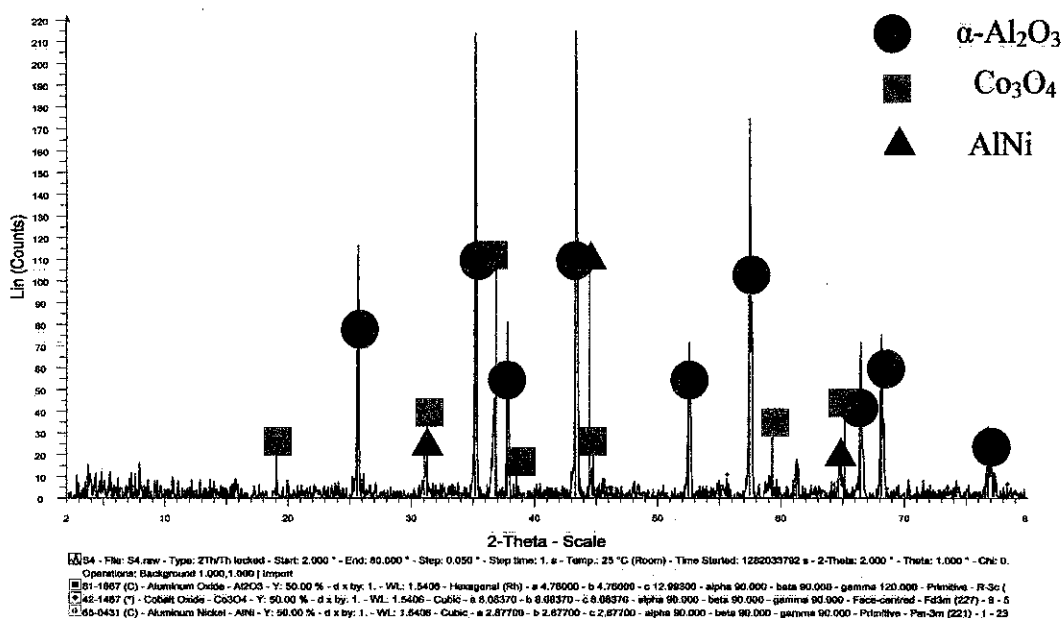


Figure 9: XRD Result for 2.5%Co2.5%Ni/Al<sub>2</sub>O<sub>3</sub> employing co-impregnation method

Figure 9 shows XRD result for Ni-Co/Al<sub>2</sub>O<sub>3</sub> (co-impregnation; 95 wt% Al<sub>2</sub>O<sub>3</sub>, 2.5 wt% Co, 2.5% Ni). Based on the graph, we can see some diffraction peaks appear at 2θ value of 26.7°, 35°, 38°, 42°, 43°, 46°, 52.5°, 58°, 60°, 61°, 66°, 68°, 70°, 74° and 78°, which match to Corundum Oxide. Besides, there are some diffraction peaks appear at 2θ value of 19°, 31°, 37°, 39°, 45°, 56°, 59°, 65°, 69°, 74°, 77°, and 78°; which match to Cobalt Oxide, Co<sub>3</sub>O<sub>4</sub>. Besides, there are some diffraction peaks appear at 2θ value of 18°, 21°, 31°, 45°, 55°, and 65°, which match to AluminumNickel, AlNi. The diffraction peaks show the presence of Corundum Oxide, Co<sub>3</sub>O<sub>4</sub>AlNi and in the sample which conforms to the claim that the sample contains Co-Ni/Al<sub>2</sub>O<sub>3</sub>. The highest intensity is shown by diffraction peak at 2θ value of 35°, 37° and 43° while the lowest intensity is shown by diffraction peak at 2θ value of 18°, 21°, 31°, 36°, 46°, 54°, 57°, 66°, and 71°. The highest intensity appears at Corundum Oxide, Nickel Oxide and Cobalt Oxide diffraction peak, which shows that more crystalline phases of all components are detected in the sample at the specified intensity.

### 4.1.7 Sample 7

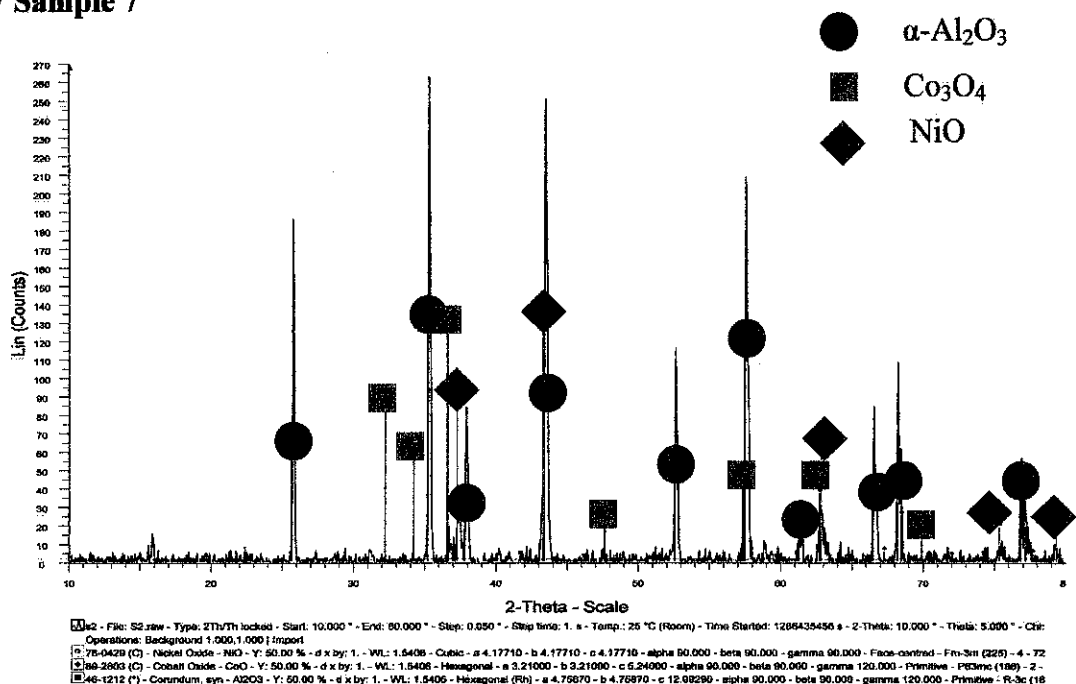


Figure 10: XRD Result for 1%Co4%Ni/Al<sub>2</sub>O<sub>3</sub> employing co-impregnation method

Figure 10 shows XRD result for Co-Ni/Al<sub>2</sub>O<sub>3</sub> (co-impregnation; 95 wt% Al<sub>2</sub>O<sub>3</sub>, 4wt% Ni, 1% Co). Based on the graph, we can see some diffraction peaks appear at 2 $\theta$  value of 26.7<sup>0</sup>, 35<sup>0</sup>, 38<sup>0</sup>, 42<sup>0</sup>, 43<sup>0</sup>, 46<sup>0</sup>, 52.5<sup>0</sup>, 58<sup>0</sup>, 60<sup>0</sup>, 61<sup>0</sup>, 66<sup>0</sup>, 68<sup>0</sup>, 70<sup>0</sup>, 74<sup>0</sup> and 78<sup>0</sup>; which match to Corundum. Besides, there are some diffraction peaks appear at 2 $\theta$  value of 19<sup>0</sup>, 31<sup>0</sup>, 37<sup>0</sup>, 39<sup>0</sup>, 45<sup>0</sup>, 56<sup>0</sup>, 59<sup>0</sup>, 65<sup>0</sup>, 69<sup>0</sup>, 74<sup>0</sup>, 77<sup>0</sup>, and 78<sup>0</sup>; which match to Cobalt Oxide, Co<sub>3</sub>O<sub>4</sub>. Besides, there are some diffraction peaks appear at 2 $\theta$  value of 18<sup>0</sup>, 21<sup>0</sup>, 31<sup>0</sup>, 36<sup>0</sup>, 37<sup>0</sup>, 43<sup>0</sup>, 47<sup>0</sup>, 54<sup>0</sup>, 57<sup>0</sup>, 63<sup>0</sup>, 66<sup>0</sup>, 71<sup>0</sup>, 75<sup>0</sup>, and 79<sup>0</sup>; which match to Nickel Oxide, NiO. The diffraction peaks show the presence of Corundum, Co<sub>3</sub>O<sub>4</sub> and NiO in the sample which conforms to the claim that the sample contains Co-Ni/Al<sub>2</sub>O<sub>3</sub>. The highest intensity is shown by diffraction peak at 2 $\theta$  value of 35<sup>0</sup>, 37<sup>0</sup> and 43<sup>0</sup> while the lowest intensity is shown by diffraction peak at 2 $\theta$  value of 42<sup>0</sup> and 46<sup>0</sup>. The highest intensity appears at Corundum Oxide, Nickel Oxide and Cobalt Oxide diffraction peak, which shows that more crystalline phases of all components are detected in the sample at the specified intensity.

#### 4.1.8 Sample 8

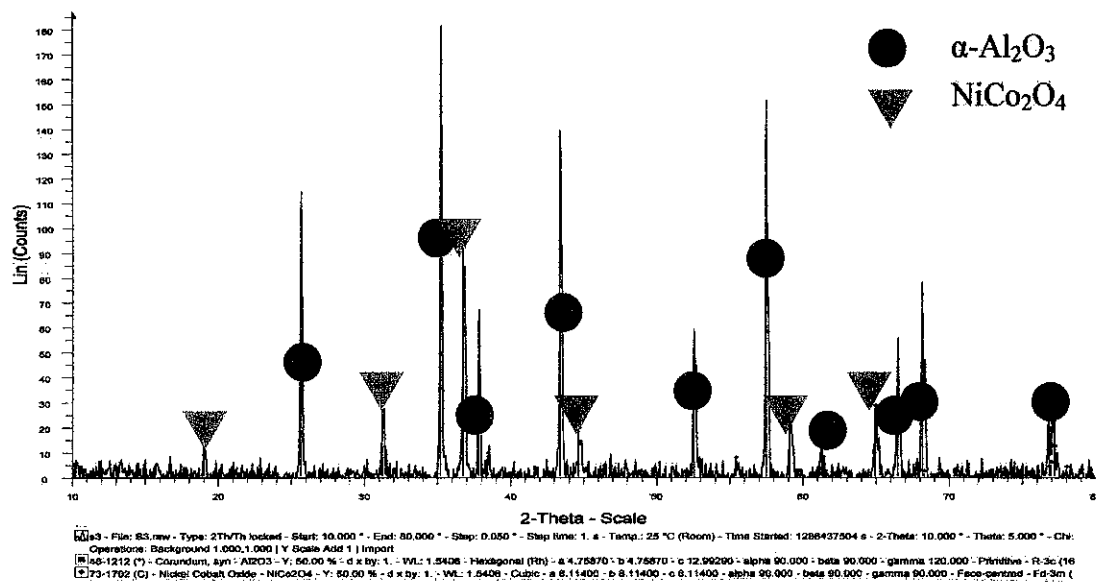


Figure 11: XRD Result for 4%Co1%Ni/Al<sub>2</sub>O<sub>3</sub>

Figure 11 shows XRD result for Co-Ni/Al<sub>2</sub>O<sub>3</sub> (co-impregnation; 95 wt% Al<sub>2</sub>O<sub>3</sub>, 4wt% Co, 1% Ni). Based on the graph, we can see some diffraction peaks appear at 2θ value of 26.7°, 35°, 38°, 42°, 43°, 46°, 52.5°, 58°, 60°, 61°, 66°, 68°, 70°, 74° and 78°. These diffraction peaks match to Corundum Oxide. Besides, there are some diffraction peaks appear at 2θ value of 18°, 31°, 37°, 38°, 45°, 49°, 55.5°, 59°, 65°, 68°, 69°, 74°, 77°, and 78°. These diffraction peaks match to Nickel Cobalt Oxide, NiCo<sub>2</sub>O<sub>4</sub>. The diffraction peaks show the presence of Corundum and NiCo<sub>2</sub>O<sub>4</sub> in the sample which conforms to the claim that the sample contains Co-Ni/Al<sub>2</sub>O<sub>3</sub>. However, there is no single Nickel Oxide (NiO) or single Cobalt Oxide (Co<sub>3</sub>O<sub>4</sub>) crystalline phase in this sample. Both NiO and Co<sub>3</sub>O<sub>4</sub> form a single phase of Nickel Cobalt Oxide, NiCo<sub>2</sub>O<sub>4</sub>. This is due to less weight percent wt% of Ni in the sample, making the presence of NiO crystalline phase alone not too significant. The highest intensity is shown by diffraction peak at 2θ value of 35°. The highest intensity appears at both Corundum Oxide and Nickel Cobalt Oxide diffraction peak, which shows that more crystalline phases of all components are detected in the sample at the specified intensity.

#### 4.1.9 Comparison of All XRD Results

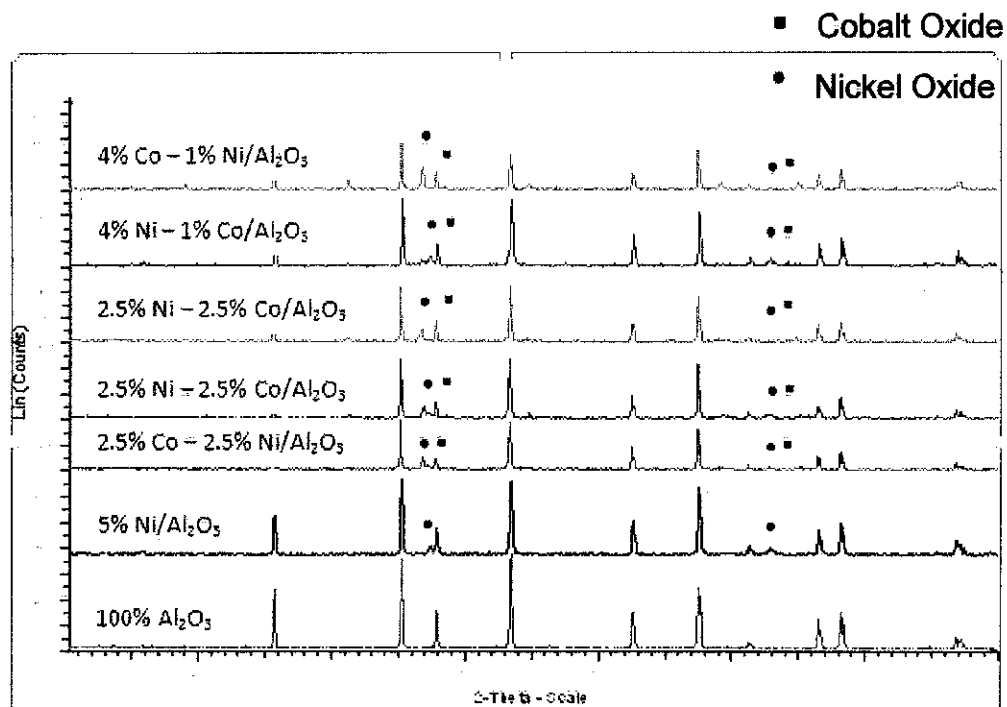


Figure 12: Comparison for XRD result for all samples

Basically, the diffraction peaks for each element in all samples of the catalyst are at the same  $2\theta$  value. There will be a new peak appearing when there is a new element in the sample. For example, in Figure 12, we can see that a new peak appear in Sample 2 containing Ni/Al<sub>2</sub>O<sub>3</sub> compared to in Sample 1 containing only Al<sub>2</sub>O<sub>3</sub>. The new peak can be seen appear at  $2\theta$  value of  $37^\circ$  and  $63^\circ$ , which match to NiO diffraction peak. This shows that a new element, Nickel (Ni) is detected in Sample 2.

For Sample 3, the new peak can be seen at  $2\theta$  value of  $36^\circ$  and it match to Co<sub>3</sub>O<sub>4</sub> diffraction peak. This shows that a new element, Cobalt (Co) is detected in Sample 3. For other samples which contain both Nickel (Ni) and Cobalt (Co), the new diffraction peaks appear at the combination of both NiO and Co<sub>3</sub>O<sub>4</sub>. However, the intensities of each diffraction peak in the samples are varies depending on the amount of crystalline phase of the elements detected in each sample. The difference in intensity of diffraction peak is due to the difference in types and position of the atoms detected in the catalyst.

#### 4.1.10 Comparison with Literature Finding

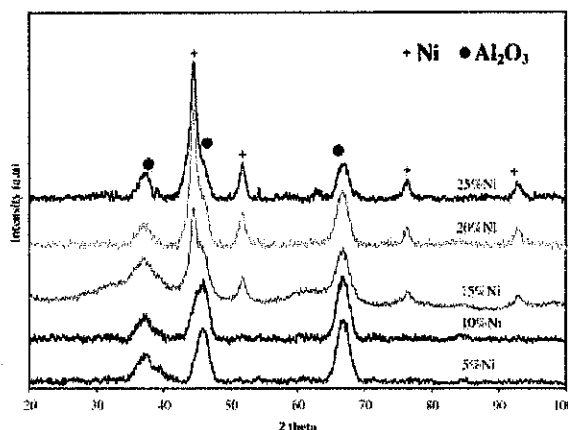




Fig. 2 - XRD spectra of reduced Ni/Al<sub>2</sub>O<sub>3</sub> catalysts.

Figure 13: XRD result Ni/Al<sub>2</sub>O<sub>3</sub> from literature review

The patterns of the diffraction peak obtained from the XRD results are comparable with the results from literature review. From Figure 13, we can see that the diffraction peak for Ni/Al<sub>2</sub>O<sub>3</sub> appear at 2θ value 37°, 45°, 49°, 54°, 66° and 75°. Comparing to the data obtained from XRD results, the 2θ values are more or less similar. Referring to Figure 7, the diffraction peaks appear at 2θ value of 26.7°, 35°, 38°, 42°, 43°, 46°, 52.5°, 58°, 60°, 61°, 66°, 68°, 70°, 74° and 78° (matching to Al<sub>2</sub>O<sub>3</sub>) and 18°, 21°, 31°, 36°, 37°, 43°, 47°, 54°, 57°, 63°, 66°, 71°, 75°, and 79° (matching to NiO).

## 4.2 SEM RESULT

Table 4: SEM results for Sample 1, Sample 2, Sample 3 and Sample 4 under 5000x magnification

Sample	5000x Magnification
<p><b>Sample 1</b> 95 wt% Al<sub>2</sub>O<sub>3</sub>, 5 wt% Ni</p>	 <p>Figure 14: SEM Result for 5%Ni/Al<sub>2</sub>O<sub>3</sub></p>
<p><b>Sample 2</b> 95 wt% Al<sub>2</sub>O<sub>3</sub>, 2.5 wt% Ni, 2.5 wt% Co (sequential impregnation method)</p>	 <p>Figure 15: SEM Result for 2.5%Ni2.5%Co/Al<sub>2</sub>O<sub>3</sub> employing sequential impregnation method</p>



**Sample 3**  
 95 wt% Al<sub>2</sub>O<sub>3</sub>, 2.5 wt%  
 Ni, 2.5 wt% Co  
 (sequential  
 impregnation method)

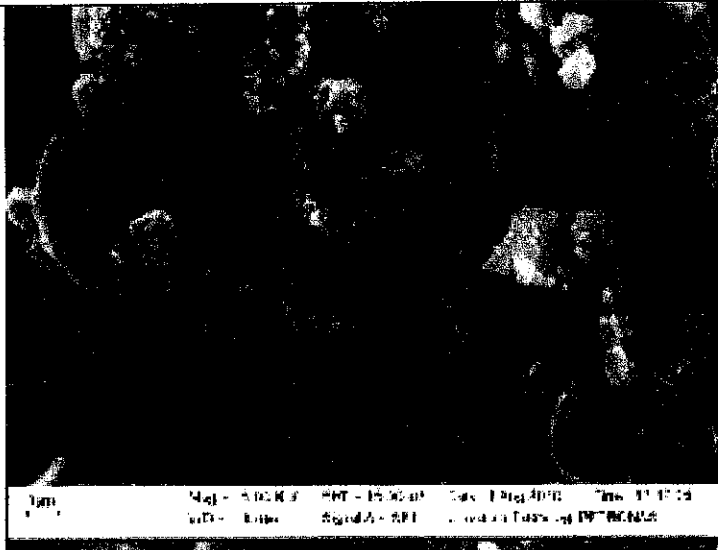


Figure 16: SEM Result for 2.5%Co2.5%Ni/Al<sub>2</sub>O<sub>3</sub> employing sequential impregnation method

**Sample 4**  
 95 wt% Al<sub>2</sub>O<sub>3</sub>, 2.5 wt%  
 Ni, 2.5 wt% Co  
 (co-impregnation  
 method)

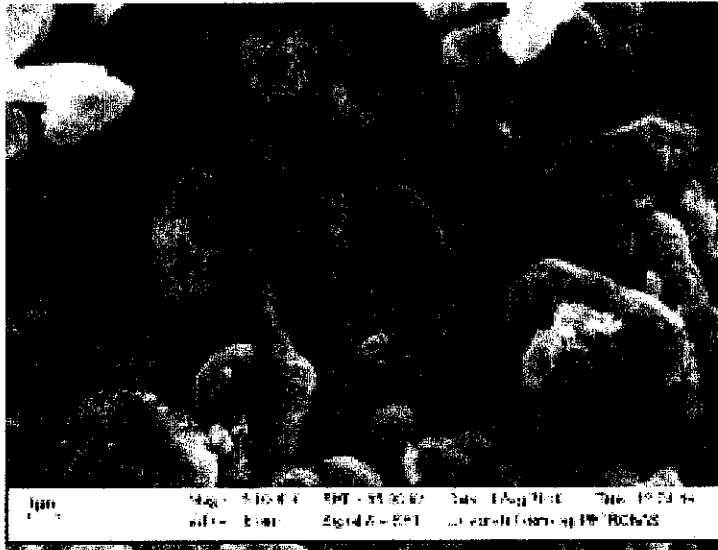
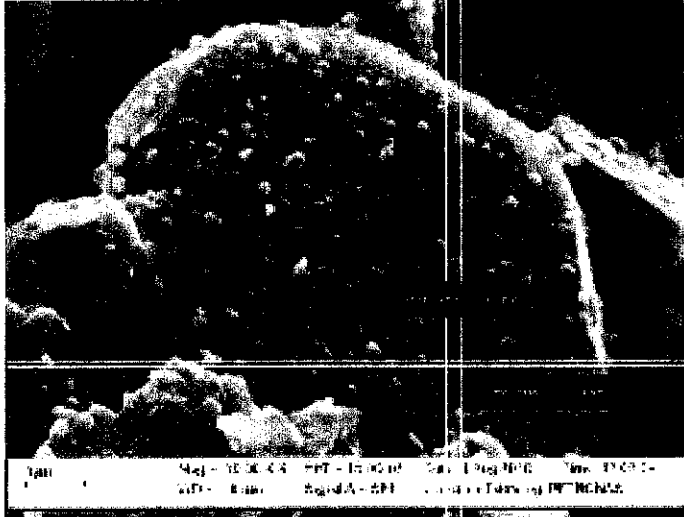
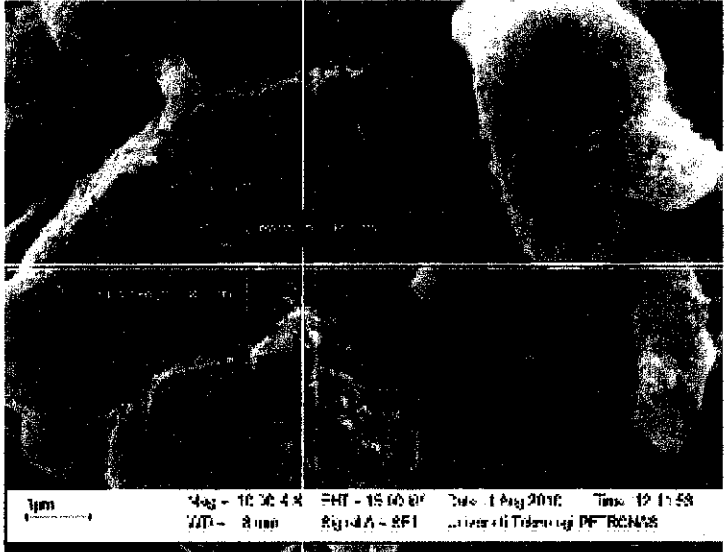


Figure 17: SEM Result for 2.5%Co2.5%Ni/Al<sub>2</sub>O<sub>3</sub> employing co-impregnation method

Table 5: SEM results for Sample 1, Sample 2, Sample 3 and Sample 4 under 10000x magnification

Sample	10000x Magnification
<p><b>Sample 1</b> 95 wt% Al<sub>2</sub>O<sub>3</sub>, 5 wt% Ni</p>	 <p>Figure 18: SEM Result for 5%Ni/Al<sub>2</sub>O<sub>3</sub></p>
<p><b>Sample 2</b> 95 wt% Al<sub>2</sub>O<sub>3</sub>, 2.5 wt% Ni, 2.5 wt% Co (sequential impregnation method)</p>	 <p>Figure 19: SEM Result for 2.5%Ni2.5%Co/Al<sub>2</sub>O<sub>3</sub> employing sequential impregnation method</p>

**Sample 3**

95 wt% Al<sub>2</sub>O<sub>3</sub>, 2.5 wt% Ni, 2.5 wt% Co  
(sequential impregnation method)

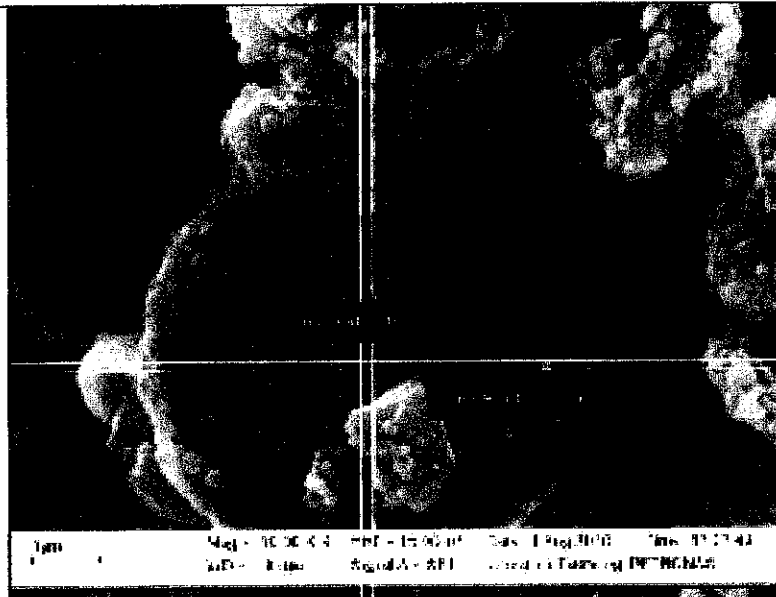


Figure 20: SEM Result for 2.5%Co2.5%Ni/Al<sub>2</sub>O<sub>3</sub> employing sequential impregnation method

**Sample 4**

95 wt% Al<sub>2</sub>O<sub>3</sub>, 2.5 wt% Ni, 2.5 wt% Co  
(co-impregnation method)

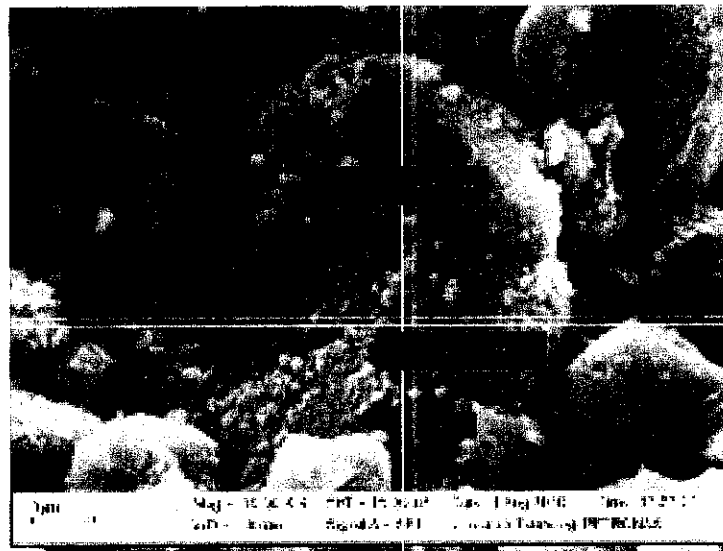


Figure 21: SEM Result for 2.5%Co2.5%Ni/Al<sub>2</sub>O<sub>3</sub> employing co-impregnation method

Based on the Figures 14 – 21, the surface morphology of each samples are quite different. The bigger particles are denoted as Al<sub>2</sub>O<sub>3</sub> while the smaller particles are metal precursors, either Cobalt or Nickel. The particles of the elements present in the samples are not uniformly distributed. Besides, the particles' shape also varies from one sample to another. This is might due to the Co-Ni ratio and the sequence of catalyst preparation method. The particle sizes of the samples are in the range of 279.1 nm of width and 78.15 nm of height.

## 4.3 EDX RESULT

### 4.3.1 Sample 1

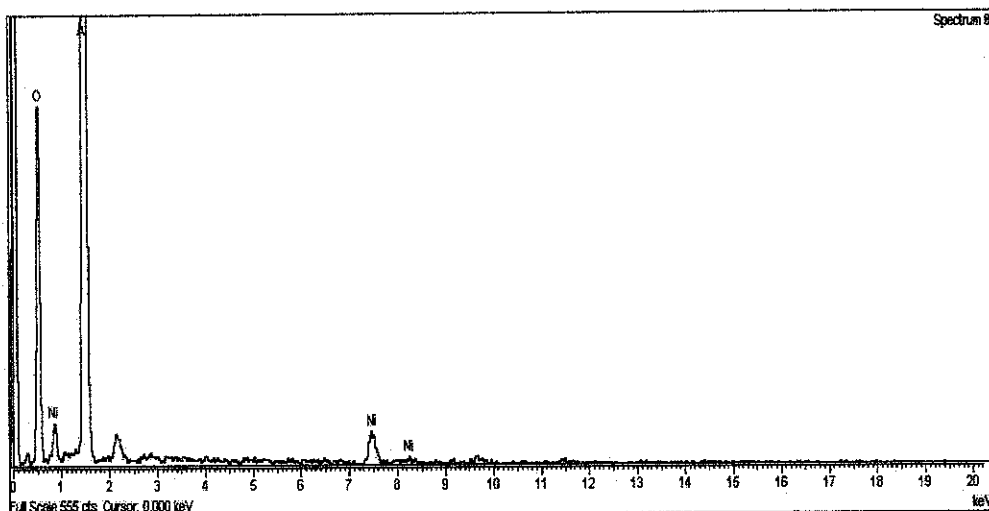


Figure 22: EDX Result for 5%Ni/Al<sub>2</sub>O<sub>3</sub>

For EDX results, they show the presence of the elements appearing in each sample. Based on EDX result, we can confirm the presence of particular element in that particular sample. By comparing EDX results with XRD results, we can see the similar detection of elements in each sample.

Based on Figure 22, EDX result show the detection of Aluminum (Al), Nickel (Ni) element, and Oxide (O) element in the sample. The higher the peak, the more elements are detected in the sample. In this sample, Aluminum (Al) element has the highest peak while Nickel (Ni) element has the lowest peak. It shows that there is more Aluminum (Al) element in this sample, compared to Nickel (Ni) element. This is to confirm that more Aluminum Oxide (Al<sub>2</sub>O<sub>3</sub>) exist in this sample compared to Nickel (Ni).

Since EDX only show the confirmation of XRD result, EDX results for other samples are attached in the appendix.

## 4.4 BET RESULT

### 4.4.1 Sample 1

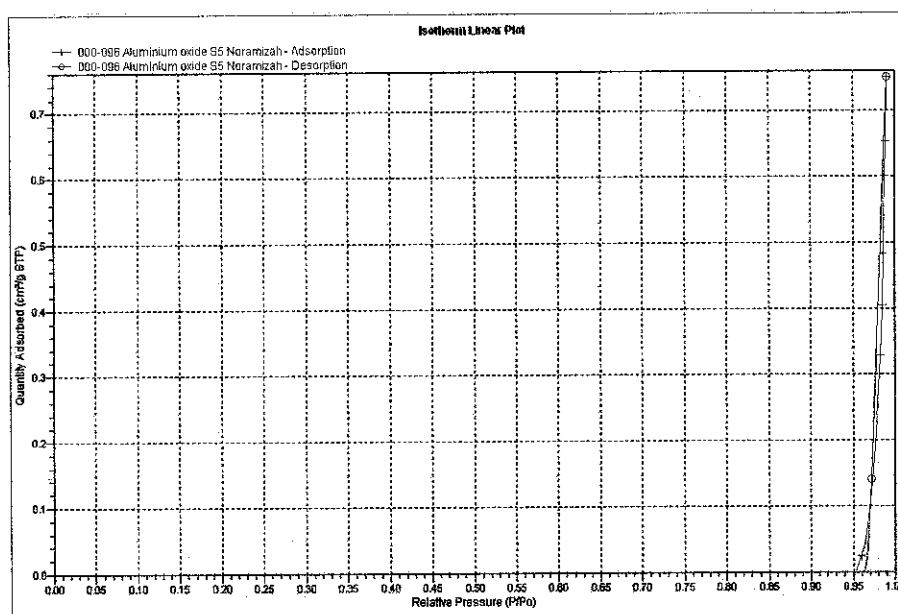


Figure 23: Isotherm Linear Plot for Aluminum Oxide

Based on Figure 26, the adsorption and desorption curve for the sample of Aluminum Oxide is quite similar with no distinct shape. The adsorption/desorption occurs at relative pressure  $P/P_0$  of 0.95 to 0.98. The higher the relative pressure, the more liquid nitrogen were adsorbed by the sample. The adsorption of liquid nitrogen starts at relative pressure of 0.95 and stop at relative pressure of 0.98. The desorption of liquid nitrogen starts at the relative pressure of 0.98, the same point of the completed adsorption. The curve continues to decrease as the relative pressure decreases and stops at relative pressure of 0.96.

Table 6 shows BET result analysis for 100%  $Al_2O_3$  including surface area, pore size and pore volume of the sample.

Table 6: BET result analysis for 100% Al<sub>2</sub>O<sub>3</sub>

<b>Surface Area</b>	
BJH Adsorption cumulative surface area of pores between 17.000 Å and 3000.000 Å width:	0.05 m <sup>2</sup> /g
<b>Pore Volume</b>	
BJH Adsorption cumulative volume of pores between 17.000 Å and 3000.000 Å width:	0.001160 cm <sup>3</sup> /g
<b>Pore Size</b>	
BJH Adsorption average pore width (4V/A):	89 nm

## 4.4.2 Sample 2

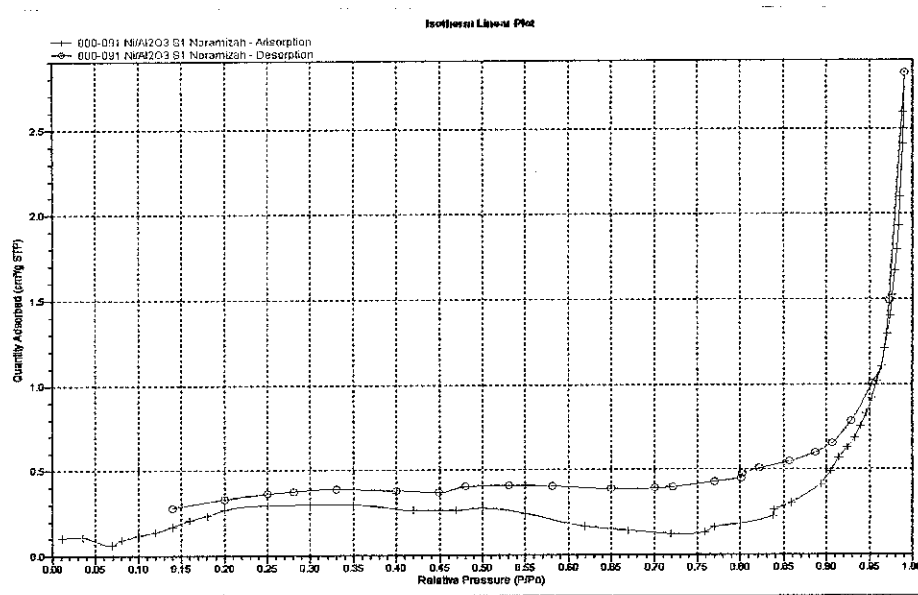


Figure 24: Isotherm Linear Plot for 5%Ni/Al<sub>2</sub>O<sub>3</sub>

Based on Figure 24, the adsorption/desorption curve for the sample of 5%Ni/Al<sub>2</sub>O<sub>3</sub> is quite similar in pattern. The shape of the curves slightly follows the Type B of Hysteresis loop on Type IV Isotherm but both the adsorption and desorption curves do not intercept. The adsorption/desorption occurs at relative pressure P/P<sub>0</sub> of 0.01 to 0.99. The adsorption of liquid nitrogen starts at relative pressure of 0.01, continue to increase and stop at relative pressure of 0.99. The desorption of liquid nitrogen starts at the relative pressure of 0.99, the same point of the completed adsorption. The curve continues to decrease as the relative pressure decreases and stops at relative pressure of 0.14.

Table 7 shows BET result analysis for 5% Ni/Al<sub>2</sub>O<sub>3</sub> including surface area, pore size and pore volume of the sample.



Table 7: BET result analysis for 5%Ni/ Al<sub>2</sub>O<sub>3</sub>

<b>Surface Area</b>	
BET surface area	4.79 m <sup>2</sup> /g
<b>Pore Volume</b>	
BJH desorption cumulative volume of pores between 17.000 Å and 3000.000 Å width:	0.0044 cm <sup>3</sup> /g
<b>Pore Size</b>	
BJH desorption average pore width (4V/A):	17.15 nm

### 4.4.3 Sample 3

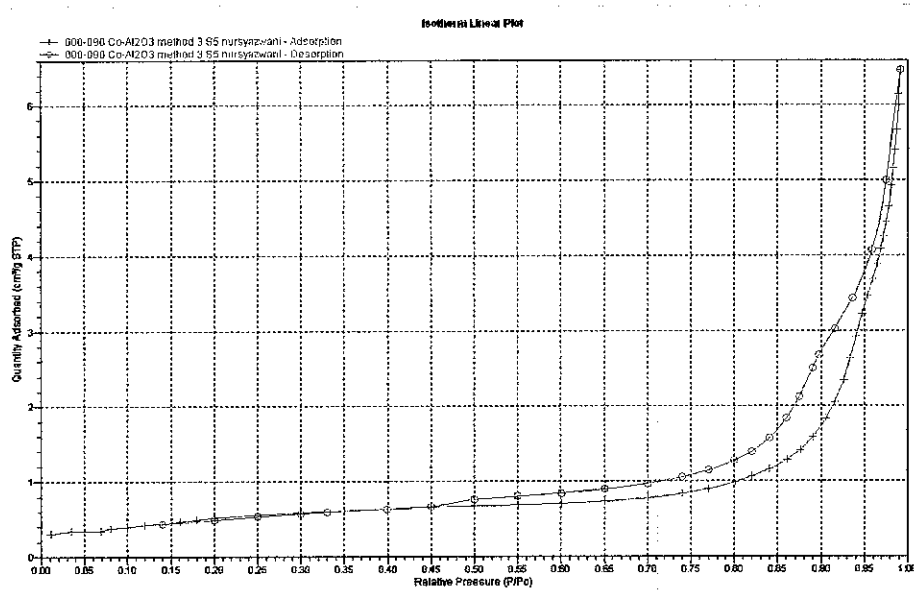


Figure 25: Isotherm Linear Plot for 5%Co/Al<sub>2</sub>O<sub>3</sub>

Based on Figure 25, the adsorption/desorption curve for the sample of 5%Co/Al<sub>2</sub>O<sub>3</sub> is quite similar in pattern. The shape of the curves fully follows the Type B of Hysteresis loop on Type IV Isotherm. The adsorption/desorption occurs at relative pressure P/P<sub>0</sub> of 0.01 to 0.99. The adsorption of liquid nitrogen starts at relative pressure of 0.01, continue to increase and stop at relative pressure of 0.99. The desorption of liquid nitrogen starts at the relative pressure of 0.99, the same point of the completed adsorption. The curve continues to decrease as the relative pressure decreases and intercept with adsorption curve at point of 0.45, then it follows the adsorption curve to decrease and stops at relative pressure of 0.14.

Table 8 shows BET result analysis for 5% Co/Al<sub>2</sub>O<sub>3</sub> including surface area, pore size and pore volume of the sample.

Table 8: BET result analysis for 5%Co/Al<sub>2</sub>O<sub>3</sub>

<b>Surface Area</b>	
BET surface area	2.42 m <sup>2</sup> /g
<b>Pore Volume</b>	
BJH desorption cumulative volume of pores between 17.000 Å and 3000.000 Å width:	0.0050 cm <sup>3</sup> /g
<b>Pore Size</b>	
BJH desorption average pore width (4V/A):	13.59 nm

#### 4.4.4 Sample 4

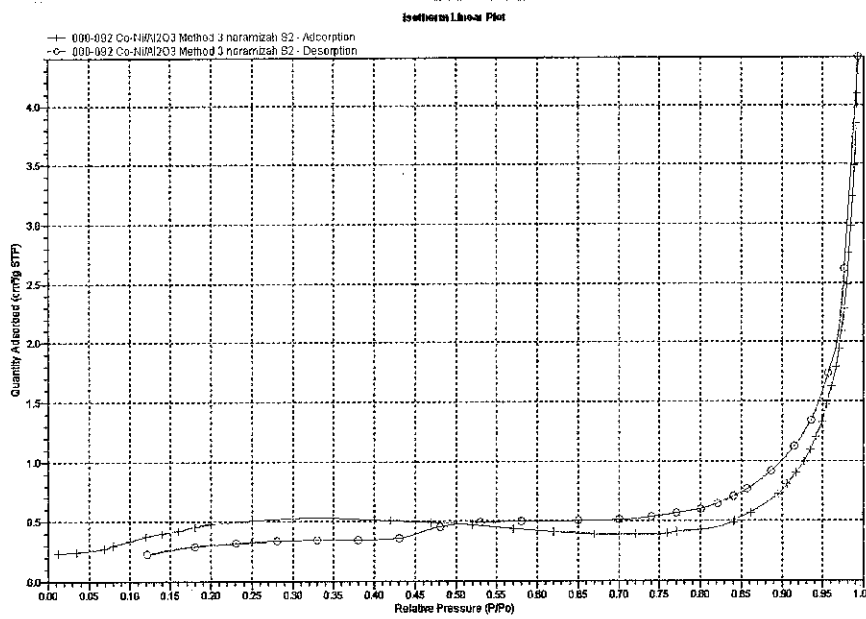


Figure 26: Isotherm Linear Plot for 2.5%Co2.5%Ni/Al<sub>2</sub>O<sub>3</sub> employing sequential method

Based on Figure 26, the adsorption/desorption curve for the sample of 2.5%Co2.5%Ni/Al<sub>2</sub>O<sub>3</sub> is quite similar in pattern. The shape of the curves slightly follows the Type B of Hysteresis loop on Type IV Isotherm, but after intercepting, both the adsorption and desorption curves emerge. The adsorption/desorption occurs at relative pressure P/P<sub>0</sub> of 0.01 to 0.99. The adsorption of liquid nitrogen starts at relative pressure of 0.01, continue to increase and stop at relative pressure of 0.99. The desorption of liquid nitrogen starts at the relative pressure of 0.99, the same point of the completed adsorption. The curve continues to decrease as the relative pressure decreases and intercept with adsorption curve at point of 0.50, then continue to decrease and stops at relative pressure of 0.14.

Table 9 shows BET result analysis for 2.5% Co2.5%Ni/Al<sub>2</sub>O<sub>3</sub> including surface area, pore size and pore volume of the sample.

Table 9: BET result analysis for 2.5%Co2.5%Ni/Al<sub>2</sub>O<sub>3</sub>

<b>Surface Area</b>	
BET surface area	1.97 m <sup>2</sup> /g
<b>Pore Volume</b>	
BJH desorption cumulative volume of pores between 17.000 Å and 3000.000 Å width:	0.0066 cm <sup>3</sup> /g
<b>Pore Size</b>	
BJH desorption average pore width (4V/A):	25.29 nm

#### 4.4.5 Sample 5

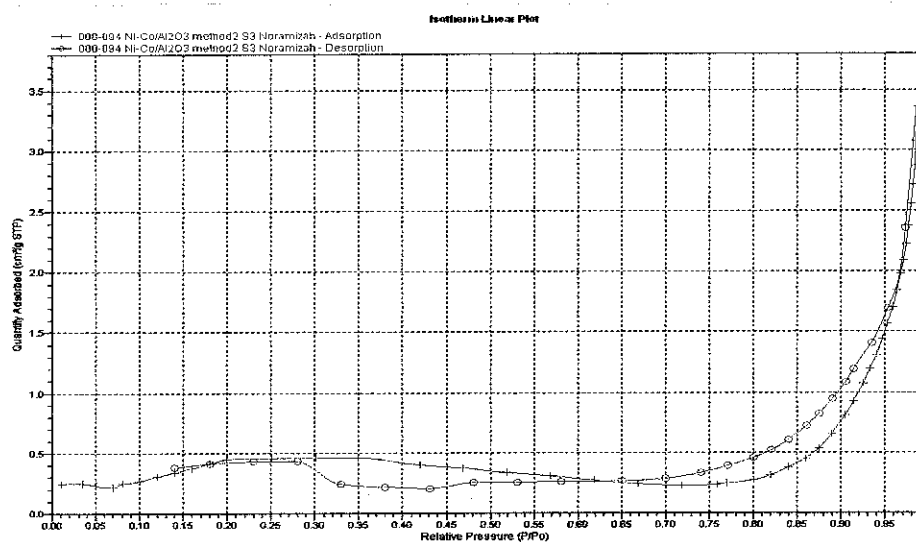


Figure 27: Isotherm Linear Plot for 2.5%Ni2.5%Co/Al<sub>2</sub>O<sub>3</sub> employing sequential method

Based on Figure 27, the adsorption/desorption curve for the sample of Ni/Al<sub>2</sub>O<sub>3</sub> is quite similar in pattern. The shape of the curves slightly follows the Type B of Hysteresis loop on Type IV Isotherm, but there are two interceptions. The adsorption/desorption occurs at relative pressure P/P<sub>0</sub> of 0.01 to 1.00. The adsorption of liquid nitrogen starts at relative pressure of 0.01, continue to increase and stop at relative pressure of 1.00. The desorption of liquid nitrogen starts at the relative pressure of 1.00, the same point of the completed adsorption. The curve continues to decrease as the relative pressure decreases and intercept with adsorption curve at point of 0.50 and continue to decrease and intercept with adsorption curve at point of 0.25, then continue to decrease and stops at relative pressure of 0.14.

Table 10 shows BET result analysis for 2.5% Ni2.5%Co/Al<sub>2</sub>O<sub>3</sub> including surface area, pore size and pore volume of the sample.

Table 10: BET result analysis for 2.5%Ni2.5%Co/Al<sub>2</sub>O<sub>3</sub> employing sequential method

<b>Surface Area</b>	
BET surface area	1.99 m <sup>2</sup> /g
<b>Pore Volume</b>	
BJH desorption cumulative volume of pores between 17.000 Å and 3000.000 Å width:	0.0058 cm <sup>3</sup> /g
<b>Pore Size</b>	
BJH desorption average pore width (4V/A):	26.94 nm

#### 4.4.6 Sample 6

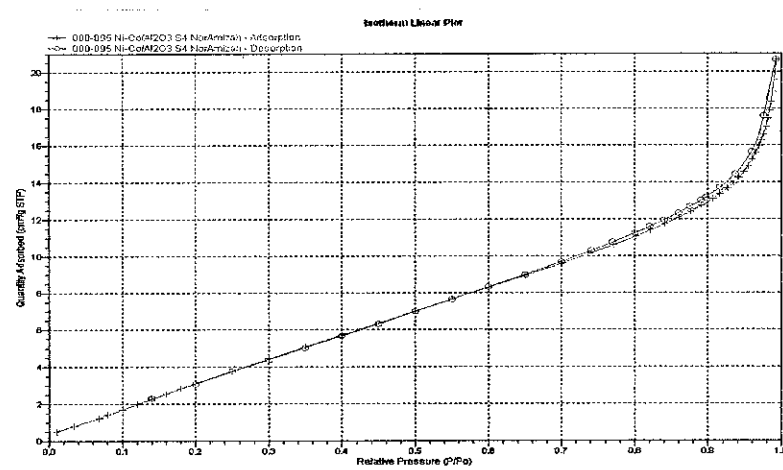


Figure 28: Isotherm Linear Plot for 2.5%Ni2.5%Co/Al<sub>2</sub>O<sub>3</sub> employing co-impregnation method

Based on Figure 28, the adsorption/desorption curve for the sample of Ni/Al<sub>2</sub>O<sub>3</sub> is quite similar in pattern. The shapes of the curves do not follow any type of Hysteresis loop on Type IV Isotherm. For both adsorption and desorption, the amount of adsorbed/desorbed increase linearly with the relative pressure before forming curves at point of 0.87. The adsorption of liquid nitrogen starts at relative pressure of 0.01, continue to increase and stop at relative pressure of 0.99. The desorption of liquid nitrogen starts at the relative pressure of 0.99, the same point of the completed adsorption, continue to decrease and stop at point of 0.01. There is no significant difference in the shape of both curves.

Table 11 shows BET result analysis for 2.5%Ni2.5%Co/Al<sub>2</sub>O<sub>3</sub> including surface area, pore size and pore volume of the sample.



Table 11: BET result analysis for 2.5%Ni2.5%Co/Al<sub>2</sub>O<sub>3</sub> employing co-impregnation method

<b>Surface Area</b>	
BET surface area	21.68 m <sup>2</sup> /g
<b>Pore Volume</b>	
BJH desorption cumulative volume of pores between 17.000 Å and 3000.000 Å width:	0.0300 cm <sup>3</sup> /g
<b>Pore Size</b>	
BJH desorption average pore width (4V/A):	6.80 nm

## **CHAPTER 5**

### **CONCLUSION**

As a conclusion, the Ni-Co ratio has significant effect to the catalyst surface morphology and diffraction peaks. Different Ni-Co ratio results in different surface morphology and diffraction peaks. XRD result shows the detection of the elements appear in the catalyst samples. The EDX result from Scanning Electron Microscopy (SEM) confirms the XRD results which also showing the elements content in the catalyst. For further work, the catalyst will be tested for steam reforming of acetic acid to investigate the performances of the catalysts upon the Co-Ni ratio.

#### **5.1 RECOMMENDATIONS**

1. Characterization of all catalysts' samples to be completed
2. All samples of catalysts need to be tested by steam reforming of acetic acid
3. All samples of catalysts need to be characterized after steam reforming of acetic acid is done.
4. The project is to be continued by next batch of FYP students.

## REFERENCES

A.C. Basagiannis, X.E. Verykios, (2006). Reforming Reactions of Acetic Acid on Nickel Catalyst over a Wide Temperature Range, *Journal of Applied Catalysis A: General*, 308 pp182–193

Francesco Pinna, (1998). Supported metal catalysts preparation, *Journal of Catalysis Today*, 41, pp129 – 137

Giovanni Perego, (1998). Characterization of heterogeneous catalysts by X-ray diffraction techniques, *Journal of Catalysis Today*, 41, 1-3, pp 251-259

Kazuhiro Takanabe, Ken-ichi Aika, Koji Inazu, Toshihide Baba, K. Seshan, Leon Lefferts, (2006). Steam reforming of acetic acid as a biomass derived oxygenate: Bi-functional pathway for hydrogen formation over Pt/ZrO<sub>2</sub> catalysts, *Journal of Catalysis*, 243, pp 263–269

Luc'ia Garcia, Richard French, Stefan Czernik, Esteban Chornet, (2000). Catalytic steam reforming of bio-oils for the production of hydrogen: effects of catalyst composition, *Journal of Applied Catalysis A: General*, 201 pp225–239

Serdar Yaman, (2003). Pyrolysis of biomass to produce fuels and chemical feedstocks, *Journal of Energy Conversion and Management*, 45, pp 651-671

Stefan Czernik, Richard French, Calvin Feik, and Esteban Chornet, (1999). *Hydrogen from Biomass via Fast Pyrolysis/Catalytic Steam Reforming Process*, Thesis, National Renewable Energy Laboratory, USA

Thomas Davidian, Nolven Guilhaume, Ce'cile Daniel, Claude Mirodatos, (2008). Continuous hydrogen production by sequential catalytic cracking of acetic acid,

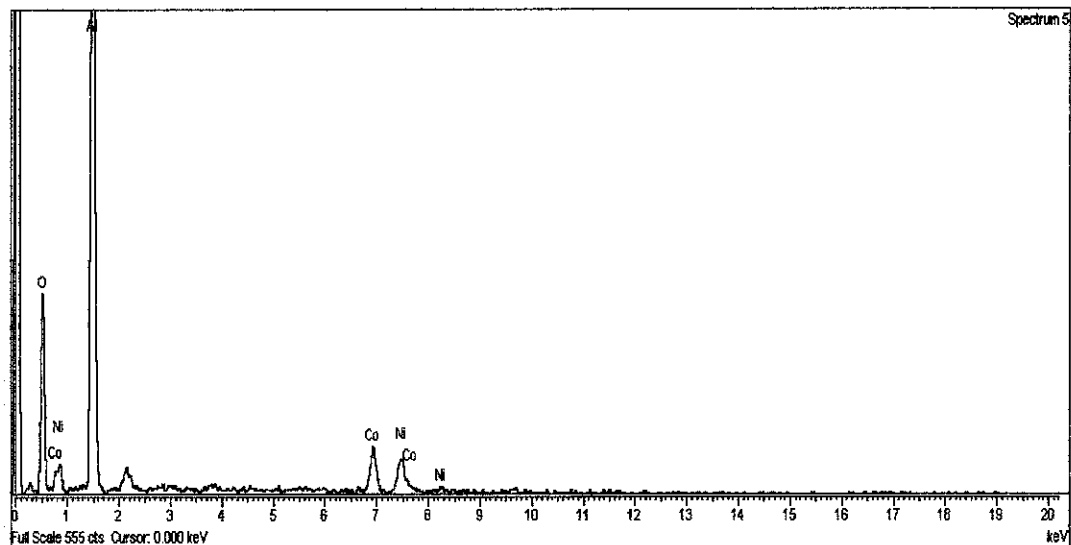
Part I - Investigation of reaction conditions and application to two parallel reactors operated cyclically, *Journal of Applied Catalysis A: General*, 335 pp64–73

Xun Hu, Gongxuan Lu, (2007). Investigation of steam reforming of acetic acid to hydrogen over Ni–Co metal catalyst, *Journal of Molecular Catalysis A: Chemical*, 261, pp 43–48

# APPENDICES

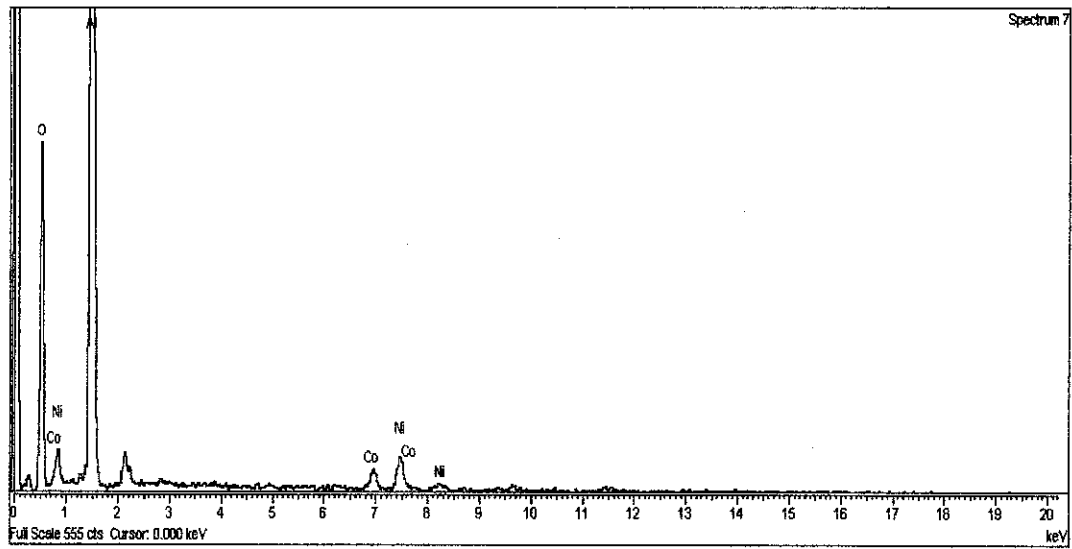
## APPENDIX 1: EDX RESULT FOR SAMPLE 2

2.5%Ni2.5%Co/Al<sub>2</sub>O<sub>3</sub> employing sequential impregnation method



## APPENDIX 2: EDX RESULT FOR SAMPLE 3

2.5%Co2.5%Ni/Al<sub>2</sub>O<sub>3</sub> employing sequential impregnation method



### APPENDIX 3: EDX RESULT FOR SAMPLE 4

2.5%Co2.5%Ni/Al<sub>2</sub>O<sub>3</sub> employing co-impregnation method

